Biosensor-based Strategies for Improving Pathway Production in *Escherichia coli*

By

Stephanie J. Doong

B.S. Chemical Engineering
Stanford University, 2014

Submitted to the Department of Chemical Engineering
in Partial Fulfillment of the Requirements for the Degree of
Doctor of Philosophy
at the
MASSACHUSETTS INSTITUTE OF TECHNOLOGY
June 2019

Signature of Author ....

Signature redacted

Stephanie J. Doong
Department of Chemical Engineering
May 7, 2019

Certified by ....

Signature redacted

Kristala L. J. Prather
Professor of Chemical Engineering
Thesis Supervisor

Accepted by ....

Signature redacted

Patrick S. Doyle
Professor of Chemical Engineering
Chairman, Committee for Graduate Students

Biosensor-based Strategies for Improving Pathway Production in *Escherichia coli*

By
Stephanie J. Doong

Abstract

Microbial production of chemicals and fuels is an attractive renewable alternative to petroleum-based processes. D-glucaric acid, a Department of Energy top value-added chemical from biomass, is a precursor to polymers such as nylons and used in detergents. An engineered metabolic pathway requiring three heterologous enzymes to convert glucose into glucaric acid in *Escherichia coli* was previously demonstrated by the Prather lab. Glucaric acid production has been shown to be limited by the two downstream enzymes *myo*-inositol-1-phosphate synthase (MIPS) and *myo*-inositol oxygenase (MIOX). This work develops and deploys a biosensor that recognizes a pathway intermediate in order to overcome both limitations.

A biosensor for *myo*-inositol (MI) was developed using the transcriptional regulator IpsA from the organism *Corynebacterium glutamicum*. A hybrid promoter was designed to enable function in the desired host organism *E. coli*. The modular design of the biosensor permitted the behavior and MI dose response to be adjusted for the pathway applications.

The *myo*-inositol biosensor was used to regulate expression of *Miox*, the enzyme that consumes *myo*-inositol, such that *Miox* was transcribed only in the presence of its substrate. Controlled expression of *Miox* led to a 2.5-fold increase in glucaric acid titer compared to the static case where *Miox* was constitutively expressed. This dynamic regulation scheme was then paired with a system that dynamically knocked down glycolysis, which independently improved glucaric acid production by relieving competition of glycolysis with MIPS, the first pathway enzyme. The layered dynamic regulation scheme improved glucaric acid production by up to 9-fold.

Next, the biosensor was used as a high-throughput screen for mutants of MIPS generated by directed evolution. The biosensor enabled a large library of MIPS to be screened by fluorescence-activated cell sorting (FACS). The screen identified MIPS mutants with up to 20% improvement in *myo*-inositol production.

This work used a biosensor to tackle two pathway limitations and improve glucaric acid production, showcasing the biosensor as a powerful metabolic engineering tool.

Acknowledgements

Contents

List of Figures

List of Tables

1. Introduction

1.1 Engineering Organisms

Microorganisms have been fermenting sugars into the essential products of wine, cheese, and bread for thousands of years. A little over 40 years ago, the introduction of recombinant DNA technology[1] rapidly expanded the accessible fermentation products beyond food. Technology to manipulate DNA has enabled scientists to modify, extend, and replace endogenous metabolic pathways for the production of desired molecules, laying the foundation for the field of metabolic engineering[2]. Metabolic engineers have coerced microbes to produce commodity chemicals and fuels from renewable feedstocks rather than petroleum (e.g. 1,3-propanediol[3] and isobutanol[4]), complex compounds that would otherwise need to be extracted from plants (e.g. artemisinin[5], opioids[6], and cannabinoids[7]), and molecules that have not been found in nature (e.g. 1,4-butanediol[8] and 1,4-butyrolactone[9]).

To create and optimize production strains, metabolic engineers employ the design – build – test cycle[10]. Genetic modifications are selected, constructed, and the resulting strains evaluated for titer, rate, and yield – the hallmark metrics of production. The results of strain evaluation are then used to guide the genetic designs for the subsequent engineering cycle.

Genetic parts and their configurations are selected in the design phase. These parts include genes encoding enzymes, forming the backbone of a production pathway. As further engineering cycles proceed, strategies to increase pathway flux, prevent product consumption, overcome endogenous regulation, relieve toxicity, and balance growth and production are applied[2,11].

These strategies may require additional parts such as protein tags, promoters, ribosome binding sites, terminators, and regulated components such as transcription factors and riboswitches. The design process has been improved with expanding databases characterizing genes and sequences (NCBI[12]), collections of known reactions and pathways (KEGG[13]), protein databases (Uniprot[14]), and computational methods to design parts (RBS calculator[15]). Algorithms such as OptKnock can predict pathways, knockouts, and enzymes exerting metabolic control[16]. There are even platforms available to compile genetic circuits into DNA sequences (CELLO[17]). These resources allow for informed design decisions and the development of more complex strategies for improving production.

The build step involves the physical assembly of DNA and construction of strains, and has been significantly simplified with dramatically reduced costs of DNA synthesis and sequencing. The continued development of numerous robust DNA assembly protocols along with an expanding plasmid repository (Addgene) have streamlined the genetic engineering process[18]. Advances in CRISPR technologies have greatly improved genome editing capabilities[19] and facilitated re-programming of many organisms (including humans[20]).

The test stage evaluates the designed strains. Strains are tested for both productivity and problems. Product titer, byproduct accumulation, biomass yield, and protein expression are examples of metrics for evaluation. Pathway bottlenecks are diagnosed with tell-tale symptoms such as side products, poor growth, and intermediate buildup. Information from the test stage

guides the next set of designs that can address pathway challenges. Recent developments in omics and analytical technologies have provided comprehensive, detailed snapshots of cellular behavior[21]. However, the test phase is still widely regarded as the bottleneck of the metabolic engineering cycle[21,22]. Conventional molecular detection methods are chromatographic, with samples and conditions tested in series. If a chemical or enzymatic assay format is available for detecting the desired product or activity, microtiter plates can increase the throughput. Yet with powerful build methods generating up to billions of variants, test capacity is far below that of build capacity. One method to address these challenges in the test stage is by developing genetic parts capable of detection: biosensors.

1.2 Biosensors as Tools for Metabolic Engineering

Adapted from natural regulatory mechanisms, genetically encoded biosensors are cellular components that perform molecular recognition. Biosensors are often re-purposed transcription factors or riboswitches that bind a molecule of interest and are engineered to regulate a phenotype-conferring reporter such as GFP.

Endogenous sensing mechanisms include riboswitches, two-component systems, and ligand responsive transcription factors[24-28]. Riboswitches are regulatory RNA molecules that rely on secondary structure to physically block or promote transcription or translation. These secondary structures are altered upon interaction with a molecule of interest[29]. Riboswitches are available for thiamine pyrophosphate[30], theophylline[31], and s-adenosyl-homocysteine[32]. Methods to engineer aptamers, RNAs that bind molecules, have been applied to construct novel biosensors for molecules of interest[29,33].

Two-component systems possess a sensing domain that binds an extracellular ligand and a kinase domain that relays a signal to a response regulator, which often controls transcription[24]. Taking advantage of the modularity of the two domains, chimeric two component systems have been built to enable an organism to sense novel particles. For example, the EnvZ-OmpR system, which responds to osmolarity in *E. coli*, has been grafted with the photoreceptor Cph1 to become responsive to light[34]. The response regulator OmpR then controlled expression of the gene *lacZ*, which breaks down the chemical X-gal to produce a dark blue color[34]. This system allowed *E. coli*

to "see" light and "print" black-and-white pictures in response. Twelve years later, that system was expanded to red-green-blue wavelengths, allowing bacteria to print in color[35].

Ligand-responsive transcription factors possess a ligand (effector) binding domain for recognizing intracellular metabolites and a DNA binding domain that regulates transcription[36,37]. Classic examples of ligand-responsive transcription factors include the commonly used *tet* and *lac* systems, where transcription factors TetR and LacI repress the *tet* and *lac* promoters respectively[38]. Transcriptional repression is relieved upon the addition of chemical inducers anhydrotetracycline (aTc) or isopropyl thiogalactopyranoside (IPTG). Other ligand-responsive transcription factors have been identified to detect metals (e.g. arsenic[39]), amino acids (e.g. lysine[40]), and pathway building blocks (e.g. malonyl-CoA[41]).

Of the various classifications of biosensors, it has been suggested that the ligand-responsive transcription factor is easiest to implement and tune compared to two-component systems and RNA-based systems[42]. Ligand-responsive transcription factors are modular and have high specificity. Many transcriptional regulators possess distinct DNA and effector binding domains, such that the residues of the effector-binding pocket may be mutated to recognize other small-molecule ligands. The absence of a known endogenous sensor for a desired compound led to the construction of synthetic biosensors via site-saturation mutagenesis,[43] chimeric transcription factor engineering by merging DNA and ligand binding domains[44,45], and de novo transcription factor design[46]. For example, AraC has been engineered to selectively recognize mevalonate,

triacetic acid lactone, ectoine, and phenolic compounds by site-saturation mutagenesis of its

effector binding domain[43,47-50].
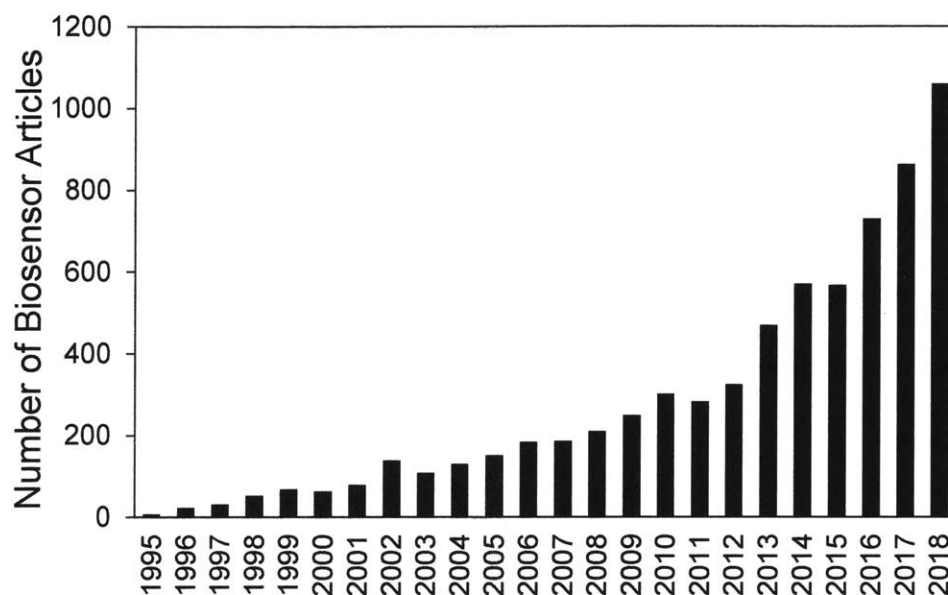
Figure 1.1. Number of publications containing keywords "biosensor" and "metabolic engineering" from Google Scholar search.

Biosensors are of considerable significance to metabolic engineers because of their capability to

serve as high-throughput screening tools for strain testing and also as regulatory genetic parts

for pathway design, particularly as key components in dynamic regulation schemes. As a result

of the multi-faceted utility of biosensors for metabolic engineers, the amount of literature

exploring genetically encoded biosensors has grown exponentially (**Figure 1.1**).

1.3 Dynamic Regulation Strategies for Pathway Improvement

Dynamic regulation is a pathway optimization strategy that draws from endogenous cellular systems. Cells possess a variety of regulation and control mechanisms in order to streamline biochemical processes and efficiently allocate resources. Studies have found that cells practice precise timing of gene expression in order to maximize product formation while minimizing resources. Upon starvation of arginine, serine, or methionine, *E. coli* initiated transcription of the upstream amino acid biosynthetic genes (*argA, serA, metA*) earlier and to a higher maximal level than the downstream genes[51]. Mathematical models found that this temporal control scheme of "just-in-time transcription" minimized the cost of enzyme expression while maximizing amino acid production[51].

Synthetic biologists have implemented such control schemes in engineered pathways with the aim of improving production. In addition to reducing expression burden and balancing metabolic fluxes, dynamic pathway regulation has been demonstrated to separate growth from production, prevent accumulation of a toxic intermediate, and combat inhibition by a downstream product[52–54]. Common dynamic regulation designs are shown in **Figure 1.2**.
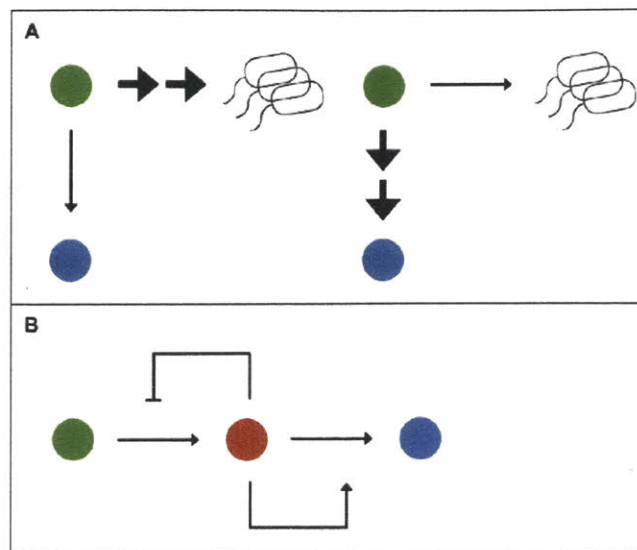
Figure 1.2. Common modes of dynamic regulation. (A) Separation of growth from production at a branch-point metabolite. (B) Dynamic pathway balancing by sensing availability of a key pathway intermediate that is toxic or used in biomass formation.

An *in silico* representation of aerobic glycerol fermentation in *E. coli* found that dynamic control balances the trade-off between growth and production and significantly improves glycerol productivity[55]. By delaying induction of glycerol kinase (*glpK*), the gene responsible for glycerol production, a growth-only phase is introduced, allowing rapid biomass formation prior to the production phase, at which point nearly all the carbon flux is shunted towards glycerol production. A similar model found that dynamically down-regulating *ackA* improved anaerobic ethanol fermentation in *E. coli*, as the static strategy of knocking out *ackA* reduced ATP availability and thus the growth rate[55].

Farmer and Liao first installed dynamic control in *E. coli* by re-directing excess carbon flux from acetate, a result of metabolism overflow during rapid growth, into the desired product lycopene. The authors used NRI, a component of the Ntr regulon, to sense acetyl-phosphate and subsequently upregulate pathway production genes *idi* and *pps* under control of the NRI-responsive *glnAp2* promoter[56]. This regulation scheme improved lycopene titers from a few mg/L to over 150 mg/L[56].

Additional pathways where dynamic regulation has had success include those for production of fatty acid ethyl esters (FAEEs)[57], fatty acids[41], and amorphadiene[58]. Production of fatty acid ethyl esters (FAEEs), a biodiesel, was improved by dynamically regulating pathway genes *pdc* and *adhB*, which generate the toxic intermediate ethanol, and *fadD* and *athA*, which siphon fatty acyl-CoAs away from cell membrane biosynthesis, hindering growth[57]. Expression of these genes was tightly controlled by an engineered promoter regulated by the fatty acid responsive transcription factor FadR[57]. This allowed the pathway genes to be induced only when sufficient concentrations of precursor fatty acids were available[57].

Fatty acid production has also been improved by balancing growth and production. FapR, a malonyl-CoA responsive transcription factor from *B. subtilis*[59], was used to balance levels of the fatty acid building block malonyl-CoA. When malonyl-CoA availability was low, FapR limited expression of fatty acid synthase, which siphons malonyl-CoA molecules into fatty acid production, and induced expression of acetyl-CoA carboxylase, which generates malonyl-CoA[41].

Conversely, when malonyl-CoA pools were high, FapR bolstered expression of the fatty acid synthase and restricted acetyl-CoA carboxylase expression[41]. The optimal balancing system resulted in a 2-fold increase in fatty acid titer[41].

In a similar balancing scheme, to combat the toxic intermediate farnesyl-pyrophosphate (FPP) in amorphadiene biosynthesis, FPP-responsive promoters were applied to control FPP production and consumption[58]. Because FPP-responsive biosensors have not been reported, and the mechanism of FPP toxicity is unknown, transcriptomics was used to identify genes that demonstrated differential changes in expression upon accumulation of FPP[58]. The promoters of these genes were then used to upregulate amorphadiene synthase and downregulate FPP biosynthesis in the presence of FPP[58].

Other strategies for dynamic control, particularly when a metabolite responsive biosensor is unavailable, include inducible transcriptional knockdown[60,61], inducible protein degradation tags[62], quorum sensing control[63,64], and CRISPR interference[65]. The numerous successful implementations of dynamic regulation demonstrate its promise as a design strategy to optimize pathway production.

1.4 High-Throughput Screening of Directed Evolution Libraries

Inspired by the natural progression of organisms across time, directed evolution is a powerful method for identifying proteins with new and improved functions. A starting template sequence is randomly mutagenized to build a library, and members of the library are screened for the desired trait. Multiple iterative rounds often ensue to reach target characteristics. Numerous mutagenesis methods are available, including error-prone PCR, DNA shuffling, and staggered extension PCR[66]. Subtilisin E was notably evolved by error-prone PCR to become hundreds of times more active than the wild-type protein in the industrial solvent dimethylformamide (DMF)[67]. Beta-lactamase was evolved by DNA shuffling to make *E. coli* 32,000 times more resistant to the antibiotic cefotaxime[68].

These tremendously successful enzyme improvements demonstrate the promise of directed evolution, especially for heterologous enzymes in engineered metabolic pathways. However, because random mutagenesis methods generate up to billions of variants, directed evolution strategies are limited by screening capacity[69]. Until recently, high-throughput screens were limited to enzymes and pathways that generate a colored or growth-requiring product. Thus, efforts have been made to use genetically encoded biosensors as a high-throughput screen for large libraries generated by directed evolution[23,70,71]. This allows cells to self-report product formation by expressing a fluorescent protein or growth-restoring gene in response to detecting the product. Whole-cell biosensors increase the test throughput by orders of magnitude (**Figure 1.3**), allowing screening throughput to only be limited by transformation efficiency. Growth-

based selections allow library members to be tested in parallel by growth on selective media. Fluorescence-based screens must be tested in series, but microfluidic technologies such as fluorescence activated cell sorting (FACS) enable single cell analysis at rates of thousands per second.
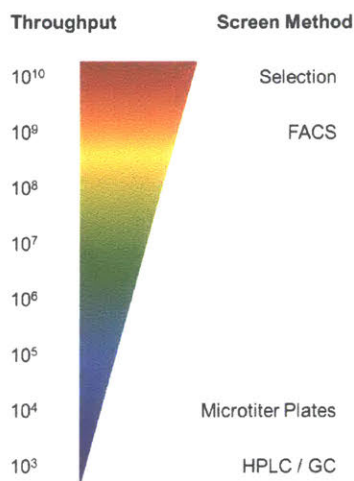
Figure 1.3. Throughput increase with biosensor-based screening. Adapted from Wang, Q., et. al. 2017 ([26]).

Recent studies in biosensor-based screening of directed evolution libraries have demonstrated success in improving pathway production. An arginine-responsive transcription factor was engineered to control expression of YFP, allowing an *argB* library in *C. glutamicum* to be screened by FACS[40]. The screen identified *argB* mutants which relieved allosteric product inhibition by 20-fold[40]. A similar lysine biosensor was used to screen libraries of pyruvate carboxylase, an upstream amino acid biosynthesis enzyme, identifying mutants that improved lysine production by up to 19%[72].

A theophylline-responsive riboswitch was attached to GFP and used to screen libraries of caffeine demethylase, which converts caffeine to theophylline, a treatment for lung problems[73]. Normally found in plants, the enzyme activity and selectivity is low in yeast, the desired host organism[73]. The FACS-based screen identified a mutant with 33-fold improvement in activity and 22-fold improvement in selectivity[73].

Biosensors that output growth-restoring genes have also been used to evolve enzymes. LysR, a transcription factor from *P. denitrificans* responsive to 3-hydroxypropionate (3-HP), a precursor to plastic polymers and acrylamide, was used to control expression of the antibiotic resistance gene *tetA* in *E. coli*[74]. This scheme permitted growth in the presence of tetracycline only when cells produced sufficient quantities of 3-HP[74]. A library of mutant alpha-ketoglutaric semialdehyde dehydrogenases was cultured in selective liquid media, which allowed the highest-producing mutants to end up as a larger fraction of the final culture population. This resulted in mutants with a 25% increase in 3-HP production[74].

When a biosensor for the pathway intermediate or product is unavailable, transcriptional regulators themselves can be engineered by evolution to bind novel ligands[43] and subsequently used in high-throughput screens. The arabinose-responsive transcription factor AraC was engineered to recognize triacetic acid lactone (TAL), a pharmaceutical precursor[48]. The TAL-responsive transcription factor controlled expression of a *lacZ* reporter and was used in a visual

plate-based screen for a library of 2-pyrone synthase mutants[48]. The screen identified mutants

with a 20-fold increase in TAL production[48]. Another AraC-derived biosensor for ectoine, a

cosmetics and pharmaceutical ingredient, was applied in a fluorescence-based screen for *ectB*,

the rate-limiting step in ectoine biosynthesis[49]. This screen found a mutant with 4-fold increase

in catalytic efficiency and 2.5-fold increase in ectoine titer[49].

1.5 D-Glucaric Acid Pathway

D-glucaric acid, a naturally occurring aldaric acid in plants and animals, is a precursor to esters and lactones, a monomer unit of biodegradable polymers such as nylons, and a chelating agent in detergents[75]. The potential uses for its many derivatives led glucaric acid to be listed in the 2004 "Top Value-Added Chemicals from Biomass" report by the US Department of Energy[75]. In 2016, glucaric acid had an annual global market of USD $500 million, which is expected to grow largely due to the increased demand for phosphate-free detergents[76]. However, the conventional chemical synthesis process involves nitric acid oxidation of glucose, a hazardous reaction that is also non-selective[75]. The environmental and safety concerns as well as the selectivity challenges can be addressed via the alternate synthesis route of bio-production.
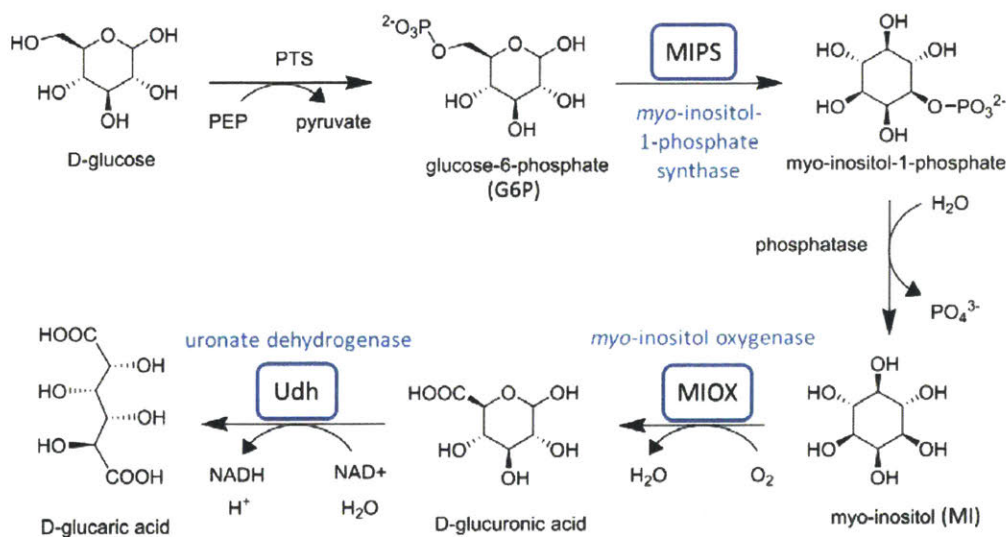
Figure 1.4. Schematic of D-glucaric acid production pathway from glucose in *E. coli*. Heterologous enzymes are shown in blue.

The Prather lab has previously developed a pathway in *E. coli* that converts glucose to glucaric acid using three heterologous enzymes (**Figure 1.4**), achieving yields of ~1 g/L glucaric acid per 10 g/L glucose[77]. The first step of the pathway uses an endogenous phosphoenolpyruvate (PEP)-dependent phosphotransferase system (PTS) to import glucose into the cell as glucose-6-phosphate (G6P). MIPS from *Saccharomyces cerevisiae* then converts G6P to *myo*-inositol-1-phosphate, which is dephosphorylated by an endogenous phosphatase (likely SuhB) to *myo*-inositol (MI). *Myo*-inositol oxygenase (MIOX) from mouse performs the oxygen-dependent conversion of MI to D-glucuronic acid. Finally, D-glucaric acid is produced from D-glucuronic acid by uronate dehydrogenase (Udh) from *Pseudomonas putida* or *Agrobacter tumefaciens*.

Of the three heterologous enzymes, Udh is by far the best-performing, with specific activity orders of magnitude above those of MIPS and MIOX[77]. Thus, most of the work to improve glucaric acid production has focused on enhancing the first two steps of the pathway. At the first step, MIPS competes with native glycolytic enzymes Pgi and Zwf for flux of G6P. Knockouts of *pgi* and *zwf* to prevent any endogenous consumption of G6P along with co-feeding of non-glucose sugars for growth allowed separation of growth from production[78]. An extension of this strategy by engineering *E. coli* to catabolize sucrose (a disaccharide of fructose and glucose) permitted growth on fructose and production from glucose[79]. To lengthen culture time and improve titers, residual glucose was shunted towards glycolysis after all fructose was consumed by dynamic control of *pgi* expression[79]. Growth-production separation has also been achieved via dynamic regulation strategies. Dynamic knockdown of glycolytic enzymes after the growth phase has been successful in improving glucaric acid titer by preventing carbon loss to biomass formation[62,63].

Substantial efforts have been made to improve the conversion of MI to glucuronic acid. The intermediate MI frequently builds up in the culture due to the low stability and specific activity of the enzyme MIOX[77]. Co-localization of MIPS and MIOX using protein scaffolds has increased MIOX specific activity as well as glucaric acid titers[80]. To improve soluble expression of MIOX, a small ubiquitin-like modifier tag was appended to the N-terminus of MIOX, which also led to increased glucaric acid production[81]. To improve the activity of MIOX, directed evolution of MIOX has been performed using a growth-based selection[81] as well as a biosensor-based screen[82]. The growth-based selection coupled high glucuronic acid producers to growth, and identified a mechanism for upregulating MI transport into the cell, but did not improve enzyme activity[81]. The biosensor-based screen used a transcription factor responsive to a glucaric acid break-down product[83] with a GFP reporter to distinguish high producers, and identified mutants of MIOX with improved specific activity[82]. Finally, as an oxygenase with an iron center, MIOX can generate reactive oxygen species that are toxic to the cell and to the enzyme itself. Expression of reactive oxygen species scavenging enzymes has been found to improved MI conversion[84].

1.6 Thesis Objectives

This work aims to improve glucaric acid production by developing a biosensor for MI to address the limiting steps in the pathway. We expand on previous dynamic pathway regulation work by layering a MI-controlled MIOX regulation system over a glycolysis knockdown scheme, simultaneously addressing the two pathway bottlenecks. We then use the biosensor as a high-throughput screen for MIPS variants, enabling identification of higher-producing mutants through a directed evolution enzyme engineering strategy. This thesis demonstrates the utility of biosensors as a genetic part for designing pathways and as a screening device for testing strains.

1.7 Thesis Organization

This thesis is organized into five chapters. Chapter 1 provides background on the metabolic engineering strategies of dynamic pathway regulation and biosensor-based evolution, and the D-glucaric acid pathway. Chapter 2 describes construction and characterization of the MI biosensor. Chapter 3 details the deployment of the MI biosensor for dynamic control of MIOX. Chapter 4 describes the use of the MI biosensor as a high-throughput screen for directed evolution of MIPS. Chapter 5 discusses the outlook of biosensors as a genetic part in metabolic engineering.

2. *myo*-Inositol Biosensor Development

Abstract

Biosensors have recently emerged as a tool for improving and optimizing engineered metabolic pathways. Sensors have been used as high-throughput screens for directed evolution of enzymes[43,48,49], autonomous induction[64], and dynamic pathway regulation[41,56,57]. Here we develop and characterize a *myo*-inositol (MI) biosensor in *E. coli*. MI, a key intermediate in the glucaric acid pathway, is natively detected in *Corynebacterium glutamicum* by the ligand-responsive transcription factor IpsA[85]. In order for the regulation system to function in *E. coli*, a hybrid promoter that fused the cognate DNA binding sequences for IpsA with a minimal *E. coli* promoter was designed. The adaptation of the MI sensor system to *E. coli* uses well-characterized and tunable genetic parts, allowing the sensor to be optimized for any particular application.

Portions of this chapter have been published in Doong, S.J., Gupta, A., and Prather, K.L.J.P. Layered dynamic regulation for improving metabolic pathway productivity in *Escherichia coli*. *Proc. Natl. Acad. Sci. U. S. A.* **115**. 2964-2969 (2018).

2.1 Introduction

Biosensors are derived from endogenous gene regulation and response mechanisms that allow for efficient adaptation to environmental changes such as carbon sources, pH, and antibiotics. These natural detection systems can be re-purposed for microbes to more effectively produce desired chemicals. Some examples include screens for directed evolution of enzymes[43,48,49], quantification of intracellular metabolites[83], autonomous induction[64], and dynamic pathway regulation[41,56,57].

In this work, a natural detection system was re-programmed as a biosensor for *myo*-inositol (MI). The ligand-responsive transcription factor, IpsA, natively regulates MI and cell wall biosynthesis in *Corynebacterium glutamicum*[85]. IpsA has been shown to bind with high specificity to MI, as well as to multiple promoter regions in the *C. glutamicum* genome[85]. In the absence of MI, IpsA binds to DNA sites, such as the promoter region of the gene encoding *myo*-inositol phosphate synthase (MIPS), and recruits RNA polymerases to activate transcription. In the presence of MI, however, IpsA binds to MI and dissociates from DNA, preventing polymerase recruitment and deactivating gene expression[85]. In *C. glutamicum*, IpsA was also found to upregulate *cg0044*, a putative ABC transporter, and downregulate inositol catabolism genes, O-succinylbenzoic acid-CoA ligase (*menE*), and iron homeostasis factors[85].

Here a tunable MI biosensor was constructed in *E. coli* from the *C. glutamicum* transcription factor IpsA and its cognate DNA-binding sequences. IpsA repressed transcription of the reporter gene *gfp* except in the presence of MI. The biosensor was characterized by GFP measurements

to determine leakiness, dynamic range, and dose response curves. The MI biosensor possessed multiple knobs for tuning, where the sensor behavior could be adjusted by the hybrid promoter configuration and the expression level of IpsA. A diverse collection of dose responsive curves was generated by adjusting these knobs, such that the MI biosensor could be tailored to fit any particular application.

2.2 Materials and Methods

2.2.1 MI Sensor Plasmid Construction

All primers used for PCR amplification of genes and promoters are found in **Table 2.3**. All plasmids used in this study are found in **Table 2.4**.

The hybrid promoter cg44 (TTTACAgtctttattgattcagtTATTATgctagcacgtgcaattttttaaaattaaaggcgtta cccaacagaggagaaatactag) was constructed by placing the IpsA binding site (underlined) from *C. glutamicum* gene *cg0044*[85] in between the -35 and -10 sites (capitalized) of promoter Bba_J23101 from the Registry of Standard Biological Parts[86]. The transcription start site is denoted in red and the RBS in green. To construct pHH-cg44-GFP, the hybrid promoter *cg44* and *gfp* were inserted into a modified form of the plasmid pHHD01K[87], which includes the rrnB terminator (ccaggcatcaaataaaacgaaaggctcagtcgaaagactgggcctttcgttttatctgttgtttgtcggtgaacgctctc) downstream of *tetR*. Briefly, *gfp* was amplified from pSB1A2-GFP[88] with primers pHH-GFP-R and cg44-RBS-GFP-F1. To incorporate the full length of the hybrid promoter *cg44* sequence, overlap extension PCR was employed by adding primer cg44-RBS-GFP-F2 to the reaction. The backbone of the modified pHHD01K was amplified with primers cg44-pHH-A and GFP-pHH-B. The backbone and insert containing *gfp* were annealed and amplified using CPEC[89]. All other hybrid promoter variants pHH-cgX-GFP, where cgX is the name of the hybrid promoter (**Figure 2.2** and **Table 2.1**), were constructed by CPEC after amplifying the insert containing *gfp* using primers GFP-C-R and cgX-F and backbone using primers GFP-C-F and cgX-R. All restriction enzymes, ligases, and polymerases were purchased from New England Biolabs (Ipswich, MA).

The gene encoding IpsA was obtained by PCR from *C. glutamicum* genomic DNA with primers EcoRI-IpsA-F and BamHI-IpsA-R, digested with EcoRI and BamHI, and ligated into the multiple cloning site of pHH-cgX-GFP to construct pHH-cg44-GFP-Ptet-ipsA. To create the tunable set of sensor plasmids, the *tet* promoter was replaced with promoters P1 through P5 (**Table 2.2**) from the Registry of Standard Biological Parts[86]. Promoters P1, P2, and P5 were inserted via CPEC using primers Px-ipsA-F and Px-pHH-R, where x = 1, 2, 5. Promoters P3 and P4 were amplified by PCR of oligos Xho1-Px-F and Kpn1-Px-R (x = 3, 4), digested with XhoI and KpnI, and ligated into the digested pHH-cg44-GFP-Ptet-ipsA backbone.

Table 2.1. List of hybrid promoters tested in **Figure 2.2**. The -35 and -10 sites are capitalized, and transcription start site denoted in red. The IpsA-binding sites, either cg3323A, cg3323B, or cg0044, are underlined.

Promoter	Sequence
cgA	TTTACAgaattgatcgatcaagcTATTATgctagcAcgtgcaatttttaaaattaaaggcgttacccaac
cgAp	TTTACAgctagctcagtcctaggTATTATgctagcAaattgatcgatcaagcttaaaggcgttacccaac
cg44	TTTACAgtctttattgattcagtTATTATgctagcAcgtgcaatttttaaaattaaaggcgttacccaac
cg44p	TTTACAgctagctcagtcctaggTATTATgctagcAtctttattgattcagtttaaaggcgttacccaac
cgA-flp	TTTACAgcttgatcgatcaattcTATTATgctagcAcgtgcaatttttaaaattaaaggcgttacccaac
cg44-flp	TTTACAactgaatcaataaagagTATTATgctagcAcgtgcaatttttaaaattaaaggcgttacccaac
cgBAdp	gcttgatcgatcaggtgttattaacTTTACAgctagctcagtcctaggTATTATgctagcAaattgatcgatcaagcttaaaggcgttacccaac
cg44dp	actgaatcaataaagagttattaacTTTACAgctagctcagtcctaggTATTATgctagcAtctttattgattcagtttaaaggcgttacccaac
cg44dc	actgaatcaataaagagttattaacTTTACAgtctttattgattcagtTATTATgctagcAcgtgcaatttttaaaattaaaggcgttacccaac
cg44cp	gttattaacTTTACAactgaatcaataaagagTATTATgctagcAtctttattgattcagtttaaaggcgttacccaac

Table 2.2. List of promoters used for driving *ipsA* expression. All promoter sequences are derived from the Registry of Standard Biological Parts[86]. The -35 and -10 sites are capitalized.

Promoter	Sequence	Parts Registry Identifier
P1	TTGACGgctagctcagtcctaggTATAGTgctagc	Bba_J23111
P2	TTTACGgctagctcagtcctaggTATAGTgctagc	Bba_J23106
P3	TTGACAgctagctcagtcctaggTATTGTgctagc	Bba_J23104
P4	TTTACGgctagctcagtcctaggTACTATgctagc	Bba_J23105
P5	TTTACGgctagctcagccctaggTATTATgctagc	Bba_J23107

2.2.2 Fluorescence Measurements

MG1655 (DE3) cells were transformed with the sensor plasmids and grown in LB (Luria Bertani) broth with 50 µg/mL kanamycin. Overnight cultures were used to inoculate 1 mL wells at 1:100 vol/vol containing LB with 50 µg/mL kanamycin on a 48-well flower plate and cultured at 30°C, shaking 1200 rpm, and 80% humidity in the BioLector (m2p Labs, Baesweiler, Germany). For variants with the *tet* promoter driving *ipsA*, 50 ng/µL anhydrotetracycline (aTc) was added to the medium. GFP fluorescence (excitation: 488 nm; emission: 520 nm) and biomass (excitation: 620 nm) were monitored continuously using LED optics for 24 hours. Experiments were performed in triplicate during three separate, identical incubation periods.

The promoter strengths of P1-P5 were measured by placing *rfp* under their control. MG1655 (DE3) cells were transformed with the plasmid series and grown in culture tubes containing 5 mL LB with 50 µg/mL kanamycin. Samples of 200 µL volume were removed 24 hours post inoculation and washed twice with 0.1 M sodium phosphate buffer (30 mM NaH_2PO_4 and 61 mM Na_2HPO_4) and centrifuged at 2000g, 4°C for 5 minutes. RFP fluorescence (excitation: 580 nm; emission: 610

nm) and optical density (absorbance at 610 nm) were measured using a Tecan Infinite 200 PRO (Männedorf, Switzerland) plate reader.

2.2.3 MI Fermentation

MG1655 (DE3) cells were transformed with the sensor plasmids and plasmid pTrc-Ino1. Cultures were grown in T12 medium (10 g/L D-glucose, 7.5 g/L yeast extract, 7.5 g/L soy peptone, 7 g/L Na_2HPO_4, 3 g/L KH_2PO_4, 0.5 g/L NaCl, 3 g/L $(NH_4)_2SO_4$, 4 mM $MgSO_4$) plus 50 µg/mL kanamycin and 100 µg/mL carbenicillin. Fermentation cultures were inoculated from overnight cultures at 1:100 vol/vol. Fermentation was carried out for 48 hours in the BioLector (30°C, 1200 rpm, 1.1 mL initial working volume). *INO1* expression was induced with 50 µM isopropyl β-D-1-thiogalactopyranoside (IPTG) at inoculation. Biomass and GFP were monitored as described above. At 24 and 48 hours post-inoculation, 100 µL culture from each well was removed, centrifuged at 3000*g*, 4°C, 5 minutes, and the supernatant retained for titer measurements. Experiments were performed in triplicate.

2.2.4 MI Quantification

Culture supernatants were analyzed by high performance liquid chromatography (HPLC) on an Agilent 1200 series instrument with an Aminex HPX-87H column. An isocratic, 25 minute method with 5 mM sulfuric acid mobile phase at a flow rate of 0.6 mL / minute was used. The column temperature was maintained at 65°C, and the refractive index detector (RID) at 35°C. The elution time for *myo*-inositol was 9.5 minutes and for glucose was 9.1 minutes.

Table 2.3. List of primers used for plasmid construction.

Name	Sequence
pHH-GFP-R	gatcttccccatcggtgatgagccagtgtgactctagta
cg44-RBS-GFP-F1	tagcacgtgcaattttttaaaattaaaggcgttacccaacagaggagaaatactagatgcg
cg44-RBS-GFP-F2	agtctttattgattcagttattatgctagcacgtgcaattttttaaa
cg44-pHH-A	gcataataactgaatcaataaagactgtaaagtcggcgatataggcgc
GFP-pHH-B	tactagagtcacactggctcatcaccgatggggaagatc
P2-IpsA-F	ctaggtatagtgctagcattcgtgcaatttttatgaggtaccgaattctcac
P2-pHH-R	cacgaatgctagcactatacctaggactgagctagccgtaaactcgagccaggcatc
P1-IpsA-F	gtcctaggtatagtgctagcattcgtgcaatttttatgaggtaccgaattctcac
P1-pHH-R	gctagcactatacctaggactgagctagccgtcaactcgagccaggcatc
P5-IpsA-F	gccctaggtattatgctagcattcgtgcaatttttatgaggtaccgaattctcac
P5-IpsA-F	gctagcataatacctagggctgagctagccgtaaactcgagccaggcatc
XhoI-P3-F	aaaaactcgagttgacagctagctcagtcctaggtattgtgctagc
KpnI-P3-R	aaaaaggtacctcataaaaattgcacgaatgctagcacaatacctaggac
XhoI-P4-F	aaaaaggtacctcataaaaattgcacgaatgctagcatagtacctaggactgag
KpnI-P4-R	aaaaactcgagctgatagctagctcagtcctagggattatgctagc
EcoRI-IpsA-F	tgcagaattcaaagaggagaaatactagatgattatgggtaggaaacaacaatacgga
BamHI-IpsA-R	agttggatccctagattggcgcaaccgtgg
cg44-flp-F	ctttacaactgaatcaataaagagtattatgctagcacgtgc
cg44p-RBS-GFP-F	tagcatctttattgattcagtttaaaggcgttacccaacagaggagaaatactagatgcg
cg44p-RBS-GFP-F2	ctagctcagtcctaggtattatgctagcatctttattgattcagtttaaagg
cgAp-RBS-GFP-F	tagcaaattgatcgatcaagcttaaaggcgttacccaacagaggagaaatactagatgcg
cgAp-RBS-GFP-F2	agtcctaggtattatgctagcaaattgatcgatcaagctt

Table 2.4. List of plasmids used in this study.

Plasmid	Genotype	Reference
pHHD01K	Empty vector, parent plasmid for sensors	90
pHH-cg44-GFP-P1-ipsA ... pHH-cg44-GFP-P5-ipsA	pHHD01K with *gfp* expressed from hybrid promoter variant cg44; *ipsA* expressed from constitutive promoters P1-P5	this study
pHH-cg44-GFP-Ptet-ipsA	pHHD01K with *gfp* expressed from hybrid promoter variant cg44; *ipsA* expressed from aTc-inducible Ptet promoter	this study
pHH-cg44p-GFP-Ptet-ipsA	same as pHH-cg44-GFP-Ptet-ipsA with IpsA binding site cg0044 located downstream of the -10 region	this study
pHH-cgA-GFP-Ptet-ipsA	pHHD01K with *gfp* expressed from hybrid promoter variant cgA, containing one of the IpsA binding sites from *C. glutamicum* gene cg3323 located between the -35 and -10 regions; *ipsA* expressed from aTc-inducible Ptet promoter	this study
pHH-cgAp-GFP-Ptet-ipsA	same as pHH-cgA-GFP-Ptet-ipsA with IpsA binding site cg3323A located downstream of the -10 region	this study
pHH-cgA-flp-GFP-Ptet-ipsA	same as pHH-cgA-GFP-Ptet-ipsA with cg3323A binding site located on opposite strand	this study
pHH-cg44-flp-GFP-Ptet-ipsA	same as pHH-cg44-GFP-Ptet-ipsA with cg0044 binding site located on opposite strand	this study
pHH-cgBAdp-GFP-Ptet-ipsA	IpsA binding site cg3323A located downstream of the -10 region and cg3323B located upstream of the -35	this study
pHH-cg44dp-GFP-Ptet-ipsA	IpsA binding site cg0044 located downstream of the -10 region and upstream of the -35	this study
pHH-cg44dc-GFP-Ptet-ipsA	IpsA binding site cg0044 located upstream of the -35 and between the -35 and -10 hexamers	this study
pHH-cg44cp-GFP-Ptet-ipsA	IpsA binding site cg0044 located downstream of the -10 and between the -35 and -10 hexamers	this study
pTrc-Ino1	pTrc99A with *S. cerevisiae* INO1	77

2.3 Results and Discussion

2.3.1 Construction and Characterization of the *myo*-Inositol Biosensor

To construct the MI biosensor, *E. coli* were engineered to express *ipsA* and its cognate promoter driving expression of a reporter gene. However, initial attempts to directly import the IpsA-regulated promoters from *C. glutamicum* into *E. coli* yielded no expression, likely because *E. coli* RNA polymerases could not recognize the foreign promoter. *E. coli* promoters, however, are well characterized[39,91], allowing simple design of a repressor-operator architecture. We engineered hybrid promoters that contained -35 and -10 regions recognizable by the native *E. coli* σ^{70} RNA polymerase, and an IpsA DNA binding site to permit IpsA-mediated transcription (**Figure 2.1**A). In this system, IpsA represses transcription from the hybrid promoter, presumably by blocking access to RNA polymerase. Binding of MI to IpsA causes the complex to unbind from DNA and transcription to proceed. This system may be used to exercise MI-inducible control of expression over any gene placed downstream of the hybrid promoter.
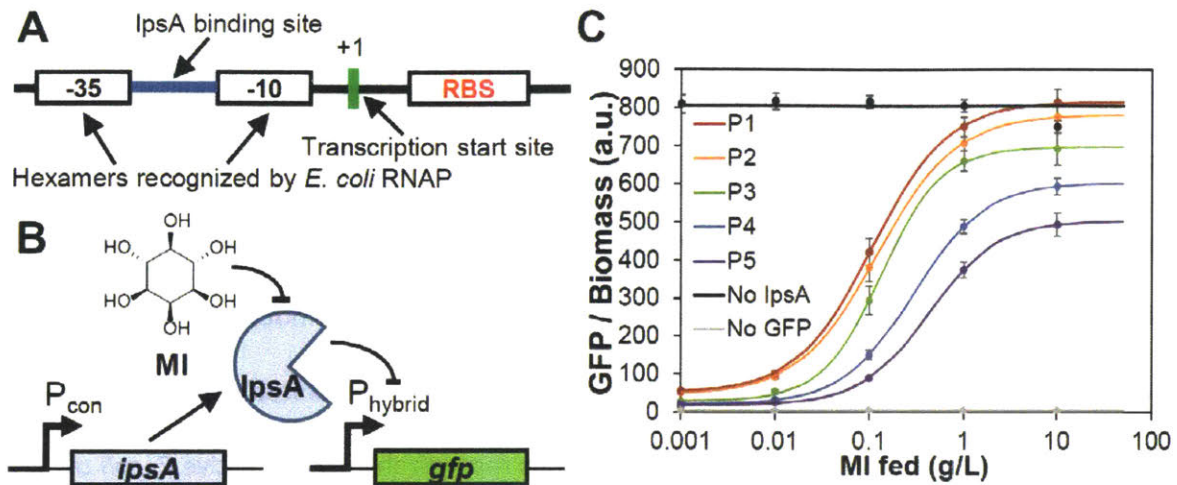
Figure 2.1. Construction and characterization of the MI biosensor. (A) Architecture of the hybrid promoter. See **Figure 2.2** for alternate hybrid promoter configurations. (B) Biosensor circuit, where a constitutive promoter expressing *ipsA* results in repression of the hybrid promoter driving *gfp* expression, and *gfp* is de-repressed in the presence of MI. (C) GFP fluorescence normalized to biomass in MG1655 (DE3) cells harboring the sensor or control plasmids as a response to MI added to LB medium. Measurements were taken 24 hours post-inoculation. Individual points with error bars represent the mean ± 1 S.D. of three replicate cultures. Data points were fitted to a dose-response transfer function to yield smooth curves. P1-P5 represent the different promoters corresponding to P$_{con}$ in (B) driving *ipsA* expression (**Figure 2.3** and **Table 2.2**). No IpsA: sensor-less plasmid expressing *gfp* from the hybrid promoter. No GFP: empty vector.

For initial characterization of the biosensor, we placed *gfp* under control of the hybrid promoter and measured the GFP fluorescence output at a range of MI concentrations (**Figure 2.1**B). Fluorescence measurements revealed a dose-dependent response to MI (**Figure 2.1**C), with increasing MI concentrations leading to increased fluorescence. Because it has been shown that placing the transcription factor binding site at different or multiple locations on the promoter may affect sensor behavior, we investigated multiple hybrid promoter variants with varying IpsA binding site sequences and locations (**Figure 2.2**). The combination of hybrid promoter variants

and *ipsA* expression levels generated a diverse collection of MI biosensors with varying dose-response behavior, providing tunable options for pathway applications.

The binding sites cg44 and cgA were obtained from the promoter regions of *C. glutamicum* genes *cg0044* and *cg3323* respectively. These binding sites were placed either between the -35 and -10 regions or downstream of the -10 region, as it has been shown that these locations lead to tight repression[91,92]. We found the hybrid promoter variant with binding site cgA placed between -35 and -10 to be very leaky, and the variant with cgA on the opposite strand to have poor dynamic range (**Figure 2.2**). The remaining variants demonstrated similar dose response curves, and the hybrid promoter with binding site cg44 placed between the -35 and -10 regions was selected for further characterization (**Figure 2.1**). For additional tunability, the amount of IpsA in the circuit was modulated by utilizing promoters of different strengths to drive *ipsA* expression (**Figure 2.3** and **Table 2.2**). As expected, increased expression of *ipsA* lowered the maximal GFP signal, and reduced the leaky expression in the absence of any MI (**Figure 2.3** and **Figure 2.4**). The presence of multiple knobs for tunability allows flexibility in reaching similar GFP levels through different circuit architectures.
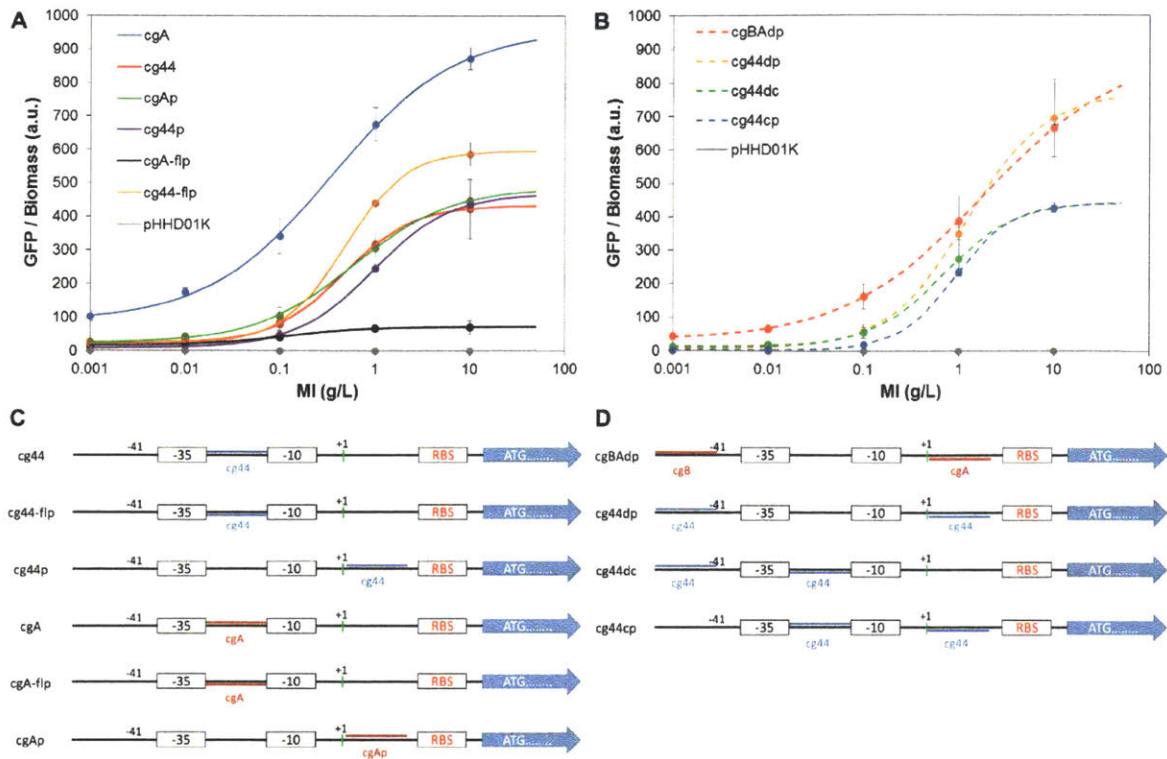
Figure 2.2. Dose response curves of hybrid promoter variants. (A) and (B) GFP fluorescence normalized to biomass in MG1655 (DE3) cells harboring sensor plasmids with hybrid promoter variants as a response to MI added to LB medium. pHHD01K represents the empty vector (no gfp) control. (C) Hybrid promoter designs for single binding site variants corresponding to dose response curves in (A). (D) Hybrid promoter designs for double binding site variants corresponding to dose response curves in (B). Sequences of the promoter variants are found in **Table 2.1**. Measurements were taken 24 hours post-inoculation. "No GFP" represents the empty vector parent plasmid used to construct the sensor plasmids, without *ipsA* expressed. Individual points with error bars represent the mean ± 1 S.D. of three replicate cultures. Data points were fitted to a dose-response transfer function to yield smooth curves.
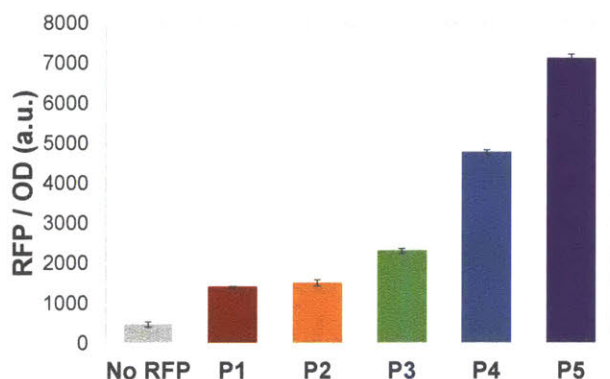
Figure 2.3. Relative strengths of the promoters (P1-P5) used to drive *ipsA* expression, as measured by RFP fluorescence. MG1655 (DE3) cells harboring the plasmids with promoters P1-P5 driving *rfp* were cultured in LB medium for 24 hours prior to fluorescence measurement. Error bars denote ± 1 S.D. from the mean of three replicate cultures.
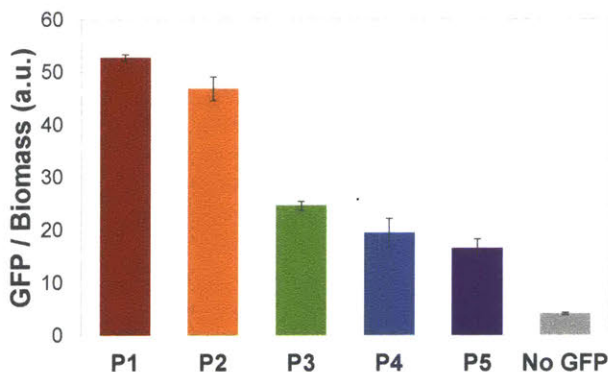
Figure 2.4. Leakage level (GFP fluorescence at 0 g/L MI) for each promoter P1-P5. MG1655 (DE3) cells harboring the sensor plasmids with hybrid promoter cg44 and promoters P1-P5 driving *ipsA* were cultured in LB medium for 24 hours prior to fluorescence measurement. "No GFP" represents the empty vector parent plasmid used to construct the sensor plasmids, without *ipsA* expressed. Error bars denote ± 1 S.D. from the mean of three replicate cultures.

In addition to evaluating the circuit with exogenously-added MI, we tested whether a response could be triggered from intracellularly produced MI. The enzyme MIPS (encoded by *INO1*), which facilitates the conversion of glucose to MI[77], was used to intracellularly produce MI from fed

glucose. Compared to the control strain harboring an empty plasmid, cells expressing *INO1* demonstrated a 16- to 55-fold increase in fluorescence, depending on the expression level of IpsA (**Figure 2.5**A). Consistent with the trends observed with exogenously-added MI in previous trials, increased *ipsA* expression decreased the endpoint fluorescence measurement, even while all strains produced approximately 1.5 g/L MI (**Figure 2.5**B). This trend suggests that a circuit with increased IpsA concentration requires more MI to achieve the same GFP output as a circuit with weaker *ipsA* expression. Furthermore, increased *ipsA* expression lengthened the amount of time required for a rise in fluorescence (**Figure 2.5**C), suggesting that de-repression of *gfp* is delayed with increasing repressor concentration, and that modulating *ipsA* expression controls the timing of switching on the reporter gene. This collection of genetic circuits (P1-P5) provides a tunable range of production responses.
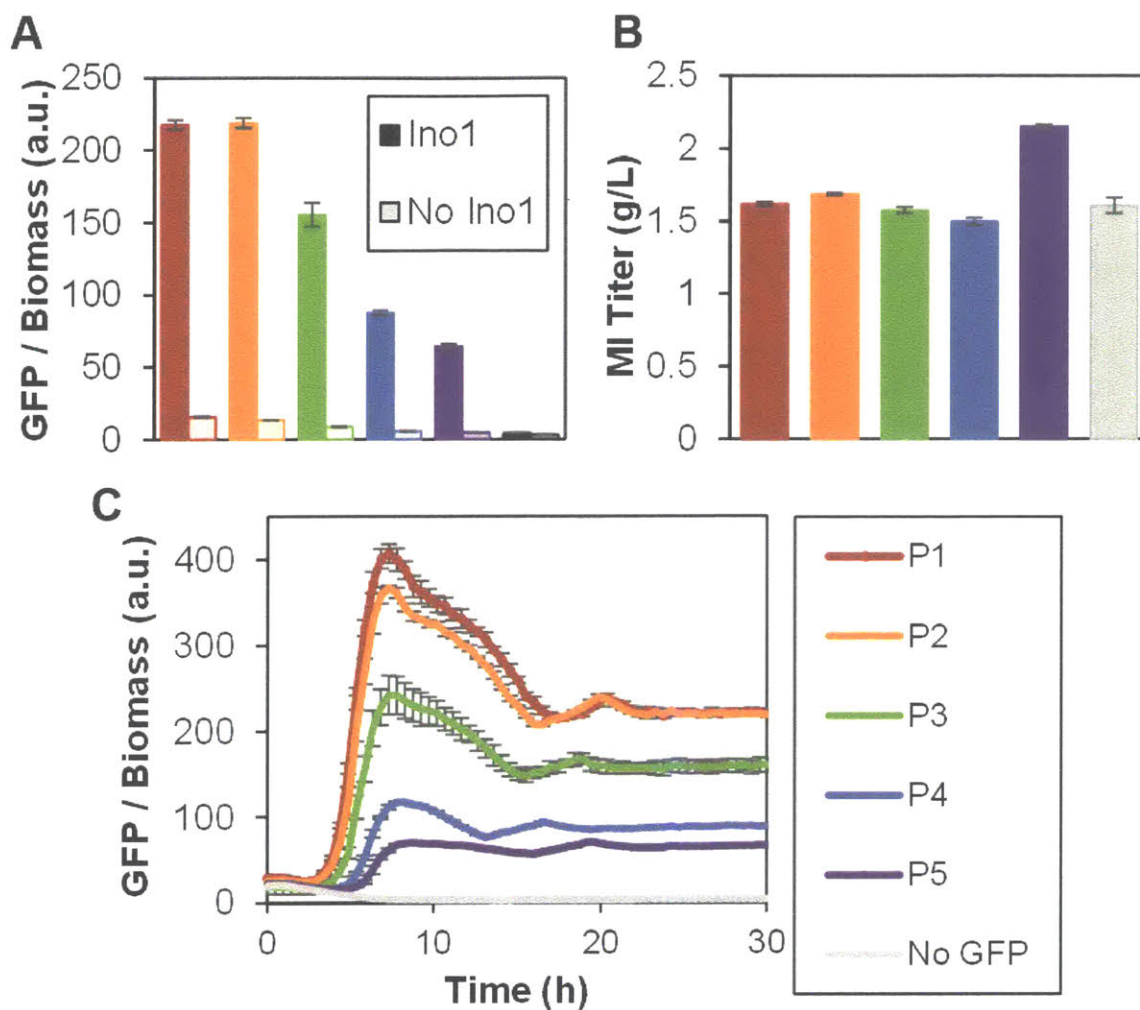
Figure 2.5. Sensor detection of MI produced from MIPS and phosphatase in MG1655 (DE3) cells. The cg44 hybrid promoter was used. (A) GFP response at 48 hours post inoculation. Expression of *INO1* in darker bars; corresponding control (empty vector in place of *INO1*) in lighter bars. (B) Corresponding MI titers at 48 hours. P1-P5 represent the different promoters driving *ipsA* expression. No GFP refers to a vector expressing *ipsA* from the *tet* promoter with a multiple cloning site in place of GFP. (C) GFP response over time with *INO1* expressed. Error bars represent ± 1 S.D. from the mean of three replicate cultures.

2.4 Conclusions

In this work we developed a MI biosensor in *E. coli* using a transcriptional regulator and cognate promoter sequences from *C. glutamicum*. The biosensor is modular and tunable, can detect extracellular MI levels between 0.01 - 10 g/L and intracellular MI produced by *E. coli* expressing *INO1*, a heterologous MI-phosphate synthase. This tunable biosensor has potential applications as a genetic part in dynamic pathway regulation (Chapter 3) and as a high-throughput screening device in directed enzyme evolution (Chapter 4). These strategies aim to improve titers, yield, and productivity in the glucaric acid pathway.

3. Dynamic Regulation of MIOX

Abstract

Microbial production of value-added chemicals from biomass is a sustainable alternative to chemical synthesis. In order to improve product titer, yield, and selectivity, the engineered pathways must be optimized. One strategy for optimization is dynamic pathway regulation, which modulates expression of pathway-relevant enzymes over the course of fermentation. Most cases, however, have used a single strategy for dynamically regulating pathway fluxes. Here we layer two orthogonal, autonomous, and tunable dynamic regulation strategies to independently modulate expression of two different enzymes to improve production of D-glucaric acid from a heterologous pathway. The first strategy uses a previously described pathway-independent quorum sensing system to dynamically knock down glycolytic flux and redirect carbon into production of glucaric acid, thereby switching cells from "growth" to "production" mode. The second strategy uses a biosensor for *myo*-inositol, an intermediate in the glucaric acid production pathway, to induce expression of a downstream enzyme upon sufficient buildup of *myo*-inositol. The latter, pathway-dependent strategy leads to a 2.5-fold increase in titer when used in isolation, and a 4-fold increase when added to a strain employing the pathway-independent regulatory system. The dual-regulation strain produces nearly 2 g/L glucaric acid, representing the highest glucaric acid titer reported to date in *E.coli* K-12 strains.

3.1 Introduction

Microbes have been engineered as renewable biochemical reactors to produce a variety of value-added compounds, such as fuels and fragrances, from low-cost substrates. After a pathway is constructed in an appropriate microbial host, it must be optimized for product titer, yield, and selectivity in order to become an economically viable process. Static strain engineering techniques for maximizing pathway productivity include balancing enzyme expression levels[93] and deleting genes expressing enzymes of competing reactions[81]. Recently, dynamic regulation has emerged as an optimization technique by implementing process control at the cellular level[52,94]. Inspired by naturally-occurring regulatory processes that allow cells to adapt to environmental changes such as temperature, osmolarity, and carbon source, dynamic regulation can be used to repurpose native regulation mechanisms to control expression of relevant enzymes.

Dynamic control can either be implemented through pathway-specific or pathway-independent strategies. Pathway-specific regulation systems control the expression of pathway enzymes in response to changes in concentration of a relevant intermediate or byproduct. Implementation of such dynamic control requires a biosensor that can detect an input change (i.e. substrate or metabolite concentration), and then actuate a response as a result of detection[42]. Thus, identification and characterization of an appropriate sensor is particularly important. For example, Farmer and Liao diverted carbon flux away from the undesired byproduct acetate towards the desired product lycopene by upregulating phosphoenolpyruvate synthase and isopentenyl diphosphate isomerase to maintain sufficient glyceraldehyde-3-phosphate (G3P) and

dimethylallyl diphosphate (DMAPP) pools upon sensing acetyl phosphate[56]. Zhang et al. used the acyl-CoA sensor FadR to repress ethanol biosynthesis genes, *adhB* and *pdc*, until sufficient accumulation of fatty acids had occurred, preventing build-up of the toxic intermediate to improve fatty acid ethyl ester production by three-fold[57]. Xu et al. increased fatty acids production by two-fold using a malonyl-CoA sensor FapR to balance the production (by acetyl-CoA carboxylase) and consumption (by fatty acids synthase) of malonyl-CoA[41].

Pathway-independent dynamic regulation strategies have also been used to improve pathway productivity. Media formulation strategies are one option in which strains are engineered with genetic circuits that respond to concentrations of critical nutrients in the medium. By tuning the concentration of these nutrients in the culture medium, the triggering time of the internal circuit can be controlled[95]. These strategies, however, may lead to unknown global metabolic effects on the cell, as concentrations of critical compounds must be modulated. In addition to media formulation, quorum sensing (QS) circuitry has also been utilized to institute pathway-independent dynamic control, as it does not rely on pathway metabolites or substrates[63,64,96]. The QS device constructed in our lab was used to knock down an enzyme involved in central carbon metabolism to boost titers of glucaric acid from a heterologous pathway. Essential pathways cannot be knocked out of the genome, but they can be dynamically downregulated to arrest growth once a desired cell density is reached[61–64,96].

We sought to develop and apply both pathway-specific and pathway-independent strategies to explore the synergies that could be achieved by layering multiple dynamic regulation devices in

the same strain, specifically in the context of glucaric acid production in *E. coli*. At the G6P branch point of the glucaric acid pathway, pathway production competes with essential glycolytic pathways which cannot be knocked out. Previous work has demonstrated that dynamically redirecting carbon flux from glycolysis to glucaric acid production at intermediate points in the fermentation can notably improve endpoint titers[63,97]. We utilized a previously implemented QS-based switch to autonomously trigger downregulation of the glycolytic enzyme Pfk-1 at different points over the course of the fermentation[63] and thereby siphon carbon into glucaric acid production. Briefly, the circuit relies on constitutive production of a small signaling molecule, 3-oxohexanoylhomoserine lactone (AHL), which is sensed by a protein activator, EsaRI70V. EsaRI70V activates its cognate promoter, P_{esaS}, in the absence of AHL. Upon sensing a certain concentration of AHL, EsaRI70V is released from P_{esaS}, thereby deactivating gene expression from P_{esaS}. By instituting differential rates of AHL production, the switching times of the circuit can be modulated. This strategy is pathway-independent, as the QS circuit does not rely on any intermediates of the glucaric acid pathway, and represents one route to improving product titers.

In addition to the G6P branch point, the key intermediate, MI, represents another point where dynamic regulation can improve production. Previous work has shown that once MIOX is expressed, its activity declines rapidly during the fermentation[77]. Thus, delaying *Miox* expression until its substrate, MI, accumulates sufficiently may delay the loss in activity and result in higher MI conversion[88]. A pathway-specific strategy was required to directly control production of the rate-controlling enzyme MIOX as a function of its substrate concentration. To implement this, a MI biosensor was constructed to sense the key intermediate, with *Miox* transcription as the

output. In this system, the MI-responsive transcriptional regulator, IpsA, from *Corynebacterium glutamicum*[85] represses an engineered promoter driving *Miox* expression until sufficient production of MI, at which point MI-bound IpsA is released from the DNA and *Miox* transcription proceeds. The timing of *Miox* expression is modulated by expressing *ipsA* at varying levels. At the optimal *Miox* expression time, glucaric acid production increased 2.5-fold compared to the unregulated *Miox* control. Thus, this strategy represents a separate route to improving glucaric acid production that is orthogonal to the pathway-independent QS strategy described above.

In order to simultaneously address the challenges at both intermediates G6P and MI, the pathway-specific MIOX control was layered over the pathway-independent Pfk-1 control. When both control strategies were implemented, the optimal combination of Pfk-1 downregulation and *Miox* expression timing resulted in the production of nearly 2 g/L glucaric acid, compared to 0.4 g/L glucaric acid produced by the strain with only Pfk-1 downregulation, at both the 250-mL shake flask and 3-L bioreactor scales.

3.2 Materials and Methods

3.2.1 Glucaric Acid Pathway Plasmid Construction

All primers used for PCR amplification of genes and promoters are found in **Table 3.1**. All plasmids

used in this study are found in **Table 3.2**.

For dynamic control of MIOX, the restriction sites SacI and NotI were first added to replace *gfp*

in pHH-cg44-GFP-P2-ipsA (see Chapter 2) via CPEC. The backbone was amplified by PCR using

primers NotI-pHH-F and SacI-pHH-R. The insert was amplified by PCR using primers pHH-NotI-

Cm-R and pHH-SacI-Cm-F. The backbone and insert were annealed and amplified by CPEC. Next,

Miox was cloned by restriction digest into the SacI and NotI sites. *Miox* was PCR amplified with

SacI-MIOX-F and NotI-MIOX-R from pTrc-MIOX[77], digested, and ligated in place of *gfp* to form

pHH-cg44-MIOX-P2-ipsA. To construct the dynamic control plasmids containing the remaining

ipsA promoters P1, P3-P5, the entire promoter plus *ipsA* sequence was digested out of the pHH-

cg44-GFP-Px-ipsA (x = 1, 3, 4, 5, see Chapter 2) using enzymes XhoI and SbfI, and ligated into the

backbone of pHH-cg44-MIOX-P2-ipsA.

The plasmid pRSFDCarb-IN-Udh, encoding enzymes MIPS and Udh, was modified from pRSFDuet-

IN-Udh[78], where the kanamycin resistance gene was swapped for carbenicillin resistance using

CPEC. The *bla* gene encoding carbenicillin resistance was PCR amplified from pET-Duet with

primers Carb-C-RSFD and Carb-N-RSFD. The pRSFDuet-IN-Udh backbone was PCR amplified with

primers RSFD-Carb-C and RSFD-Carb-N. The insert and backbone were annealed and amplified

via CPEC. All restriction enzymes, ligases, and polymerases were purchased from New England

Biolabs (Ipswich, MA).

Table 3.1. List of primers used for plasmid construction in this study.

Name	Sequence
NotI-pHH-F	gcggccgctactagagccaggcatcaaat
SacI-pHH-R	gagctctctcctctgttgggtaacgc
pHH-NotI-CAT-R	ctggctctagtagcggccgcttacgccccgccctg
pHH-SacI-CAT-F	cccaacagaggagagagctcatggagaaaaaaatcactggatatacc
SacI-MIOX-F	aaaaagagctcatgaaagttgatgttggtcctg
NotI-MIOX-R	aaaaagcggccgcttaccaggacagggtgc
Carb-C-RSFD	gcctcactgattaagcattggtaagaattaattcatgagcggatacat
Carb-N-RSFD	gacacggaaatgttgaatactcatactcttccttttttcaatattattgaagc
RSFD-Carb-C	atgtatccgctcatgaattaattcttaccaatgcttaatcagtgaggc
RSFD-Carb-N	gcttcaataatattgaaaaaggaagagtatgagtattcaacatttccgtgtc

Table 3.2. List of plasmids used in this study.

Plasmid	Genotype	Reference
pHH-cg44-MIOX-P1-ipsA ... pHH-cg44-MIOX-P5-ipsA	pHHD01K with *Miox* expressed from hybrid promoter; *ipsA* expressed from constitutive promoters P1-P5	this study
pRSFDCarb-IN-Udh	pRSFDuet with carbenicillin resistance in place of kanamycin resistance, *S. cerevisiae INO1*, and *A. tumefaciens udh*	this study
pHH-cg44-P2-ipsA	pHH-cg44-GFP-P2-ipsA with multiple cloning site in place of *gfp*	this study
pHH-cg44-MIOX	pHHD01K with *Miox* expressed from hybrid promoter	this study
pHH-J101-MIOX-P2-ipsA	pHH-cg44-MIOX-P2-ipsA with constitutive (unregulated) promoter J23101 in place of hybrid promoter cg44	this study

3.2.2 Strain Construction

All strains (**Table 3.3**) were constructed as described in Gupta, et. al 2017[63].

Table 3.3. List of strains used in this study.

Strain Name	Genotype	Description	Reference
	MG1655 (DE3) *ΔuxaC ΔgudD*	DE3 lysogen and *uxaC, gudD* knockouts	81
IB1379GA	MG1655 (DE3) *ΔendA Δzwf ΔPfkB ΔuxaC ΔgudD*	DE3 lysogen and *uxaC, gudD* knockouts Wildtype *pfkA*	62
L19GA	MG1655(DE3) *ΔendA Δzwf ΔpfkB ΔuxaC ΔgudD pfkA::PesaS-pfkA(LAA) HK022::104-esaRI170V 186(O)::**apFAB295-apFAB699**-esaI*	IB1379GA + *pfkA* driven by P_{esas} promoter + *esaI* driven by selected promoter and RBS sequence with predicted strength 1.7%	63
L24GA	MG1655(DE3) *ΔendA Δzwf ΔpfkB ΔuxaC ΔgudD pfkA::PesaS-pfkA(LAA) HK022::104-esaRI170V 186(O)::**apFAB296-apFAB700**-esaI*	L19GA with predicted strength 4.8%	63
L31GA	MG1655(DE3) *ΔendA Δzwf ΔpfkB ΔuxaC ΔgudD pfkA::PesaS-pfkA(LAA) HK022::104-esaRI170V 186(O)::**apFAB65-apFAB700**-esaI*	L19GA with predicted strength 1.2%	63

3.2.3 Glucaric acid Fermentation

Strains MG1655 (DE3), IB1379GA, L19GA, L24GA, or L31GA (**Table 3.3**) were transformed with the MIOX regulation plasmids and pRSFDCarb-IN-Udh. Overnight cultures were used to inoculate 30 mL starter cultures at approximately 1:50 vol/vol in T12 medium with 10 g/L glucose (see Chapter 2, Methods). Starter cultures were incubated for 4-8 hours, until mid-exponential phase,

and used to inoculate fermentation cultures (T12 medium with 10 g/L glucose) at a target OD_{600} (optical density measured at 600 nm) of 0.05. The 50 mL fermentation cultures were incubated for 72 hours in 250 mL baffled shake flasks at 30°C, 250 rpm and 80% humidity. *INO1* and *udh* expression were induced with 100 μM IPTG upon inoculation of the fermentation cultures. 1.4 mL samples were removed every 24 hours for OD_{600} measurements, and centrifuged at 10,000*g*, room temperature for 10 minutes to obtain supernatants for titer measurements. Experiments were performed in triplicate.

3.2.4   Bioreactor Fermentation

Overnight cultures in T12 medium with 10 g/L glucose were used to inoculate 50 mL seed cultures in 250 mL baffled shake flasks and incubated at 30°C, 250 rpm, 80% humidity for ~8 hours. Seed cultures were then used to inoculate the bioreactor (1 L working volume) at OD_{600} = 0.05. The pH was controlled at 7 using 4 M NaOH and 4 M HCl solutions. DO was controlled at 35% of maximum saturation by agitation rate (minimum 250 rpm) and constant air sparging at 1 L per minute. Batch fermentation was carried out for 72 hours, with 5 mL samples removed every 24 hours for optical density and titer measurements as described for shake flasks.

3.2.5   Glucaric acid and MI Quantification

Supernatants were analyzed by high performance liquid chromatography (HPLC) on an Agilent 1200 series instrument with an Aminex HPX-87H column. An isocratic, 25 minute method with 5 mM sulfuric acid mobile phase at a flow rate of 0.6 mL / minute was used. The column temperature was maintained at 65°C, and the refractive index detector (RID) at 35°C. The elution

times for relevant species are as follows: glucaric acid (7.9 minutes), *myo*-inositol (9.5 minutes), glucose (9.1 minutes).

3.2.6   Quantification of mRNA Levels

Miox transcript levels were quantified using quantitative RT-PCR of mRNA isolated from culture samples. Samples were collected at the equivalent of 1 OD_{600} per 1 mL, centrifuged at 3000 rpm for 10 minutes to pellet, re-suspended in 600 μL RNA Protect (Qiagen), and stored at -80°C until mRNA extraction. To lyse the cells, samples were thawed at room temperature, centrifuged at 3000 rpm for 5 minutes, re-suspended in 100 μL 1 mg/mL lysozyme in TE Buffer (10 mM Tris-HCl at pH 8.0, 1 mM EDTA), and vortexed vigorously for 10 minutes. Total mRNA extraction of the lysed pellets was performed following the illustra RNAspin Mini Kit protocol (GE Healthcare Life Sciences). Extracted mRNA was treated with DNAseI (TURBO DNA-free Kit, Life Technologies) to remove any genomic DNA. Purified mRNA concentrations were quantified with the Nanodrop 2000 (Thermo Scientific). cDNA synthesis was performed with the QuantiTect Reverse Transcription Kit (Qiagen), with 100 ng/μL total mRNA added per cDNA synthesis reaction. Quantitative PCR reactions (25 μL total) were set up as follows: 12.5 μL 2X Brilliant II SYBR qPCR High ROX Master Mix (Agilent Technologies), 0.5 μL each primer, 9.5 μL water, and 2 μL cDNA. Amplification was performed with the ABI 7300 Real Time PCR System (Applied Biosystems) at the following cycle conditions: initial incubation at 95 °C for 10 min, followed by 40 cycles at 95 °C for 30 s and 60 °C for 1 min. Threshold cycle (Ct) values were determined automatically by the ABI system software. Fold differences in *Miox* transcript levels were calculated between each sample and its respective initial time point value.

3.2.7   Statistics

When relevant, paired two-tailed student t-tests were performed to demonstrate statistically significant differences between data points. Error propagation was conducted to estimate the uncertainty on the fold changes in titer.

3.3   Results and Discussion

3.3.1   Dynamic Regulation of the Glucaric acid Pathway by Controlling MIOX

We implemented MI-dependent dynamic control of MIOX in the glucaric acid pathway by using

the circuit to control *Miox* expression in response to MI concentration. As MIOX is an unstable

enzyme whose activity drops rapidly within the first 24 hours of fermentation[77], we sought to

control the timing of *Miox* expression in order to optimize the window of its maximal activity.

Delaying *Miox* expression until a larger pool of MI has accumulated may boost enzyme activity

and pathway productivity[88]. In the IpsA-based circuit, the transcription rate of *Miox* is a joint

function of MI and IpsA concentration, and expression of *Miox* is delayed until sufficient MI is

produced. Glucaric acid production was evaluated in strains in which the genes *gudD* and *uxaC*,

encoding for enzymes that metabolize glucaric acid and its intermediates, were deleted[81]. These

trials showed that delayed *Miox* expression improved glucaric acid titers up to 2.5 ± 0.084-fold

compared to the constitutively-expressed *Miox* control (**Figure 3.1**A). These trends in production

were consistent at 24 and 48 h (**Figure 3.2**). Strain P4 produced the highest titer, likely because

the P4 circuit resulted in optimal timing of *Miox* expression. Strain P1 permitted expression of

Miox too early in the fermentation, leading to MIOX instability and lower conversion, whereas

P5 delayed *Miox* expression for too long, with insufficient time for conversion of MI. The trends

in MI buildup correspond to the delays in *Miox* expression: increased *ipsA* expression allowed

increased MI buildup before expression of *Miox* (**Figure 3.1**B).
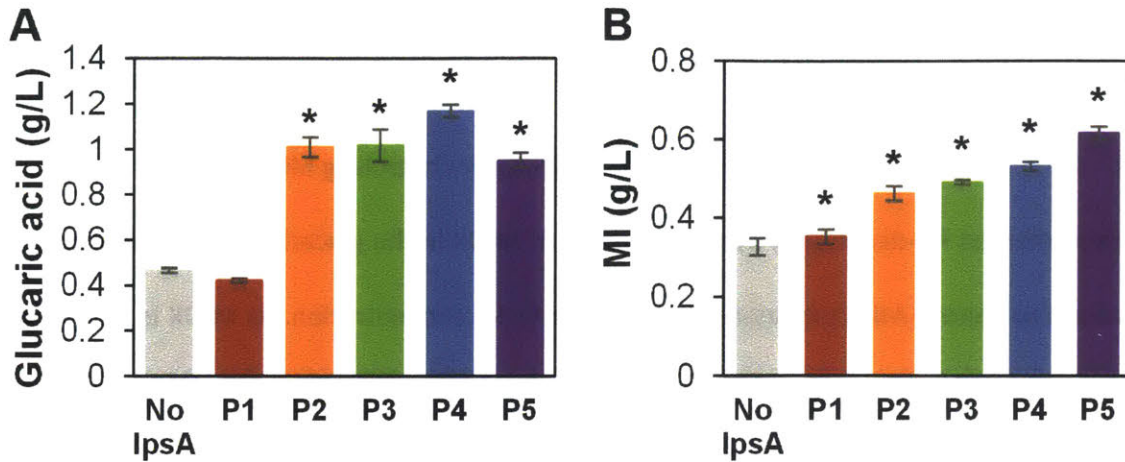
Figure 3.1. Final titers at 72 hours of (A) glucaric acid and (B) MI from MI-controlled expression of *Miox*. Production in MG1655 (DE3) Δ*gudD* Δ*uxaC*. IpsA is expressed from promoters P1-P5. No IpsA: constitutive (unregulated) *Miox* expression. Error bars represent ± 1 S.D. from the mean of three replicate flasks. *Denotes p < 0.01 compared to the No IpsA control by two-tailed t-test.
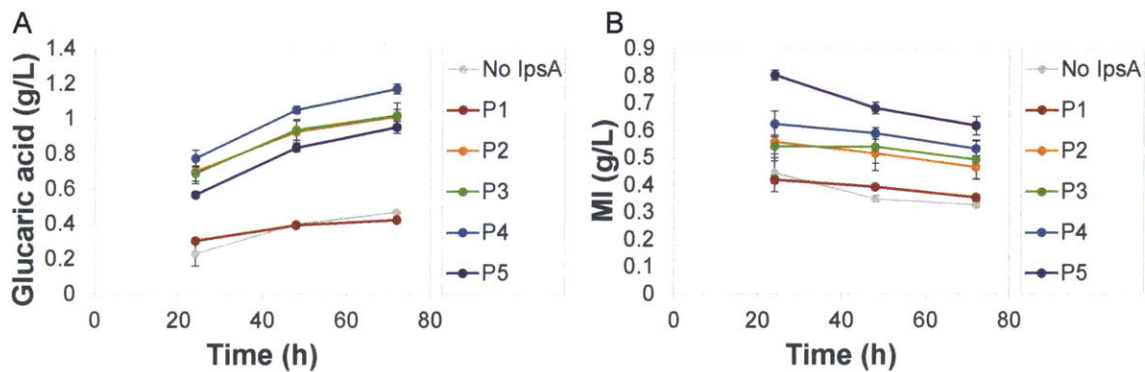
Figure 3.2. Production time course of (A) glucaric acid and (B) MI from MI-controlled expression of *Miox*. Data corresponds to that from **Figure 3.1**. IpsA is expressed from promoters P1-P5. No IpsA: constitutive (unregulated) *Miox* expression. Error bars represent ± 1 S.D. from the mean of three replicate flasks.

To confirm that repression of *Miox* by IpsA is relieved upon the production of MI, we performed qRT-PCR with two of the dynamically regulated strains to demonstrate changes in *Miox* mRNA levels over time (**Figure 3.3**). Two control strains were implemented to demonstrate static expression levels of MIOX: "No IpsA," where *Miox* is constitutively transcribed from the hybrid promoter, and "No Ino1," where MI is not produced, leading to constant repression of *Miox* by *ipsA* expressed from promoter P5. As expected, strains with promoters P2 and P5 expressing *ipsA* exhibited up to approximately 20- and 50- fold increases in *Miox* transcript levels, indicating significant de-repression of *Miox* over time, while static strains "No IpsA" and "No Ino1" did not exhibit any changes in *Miox* transcript levels. The strain with P5 exhibited a larger fold increase than P2 likely because the stronger P5 promoter is less leaky and has greater repression of *Miox* at initial times, with a P2 to P5 transcript level ratio of 5.45 ± 1.89 at the initial time point.
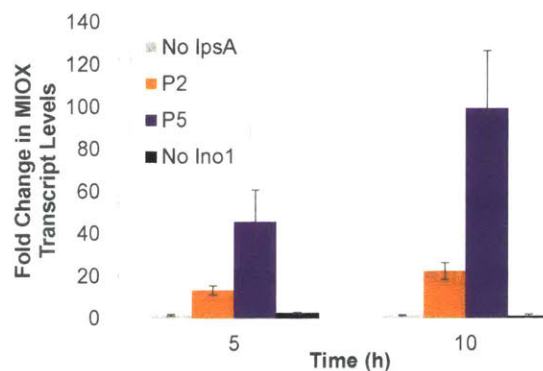
Figure 3.3. Fold change of *Miox* transcript levels over time. mRNA levels at 5 and 10 hours post-inoculation for MG1655 (DE3) ΔuxaC ΔgudD as measured by qRT-PCR. Values reported as the fold change over the initial time point for each strain. IpsA is expressed from promoters P2 and P5. No IpsA: constitutive Miox control. No Ino1: no MI production control, which ensures continuous repression of *Miox*. Error bars represent ± 1 S.D. from three replicate flasks.
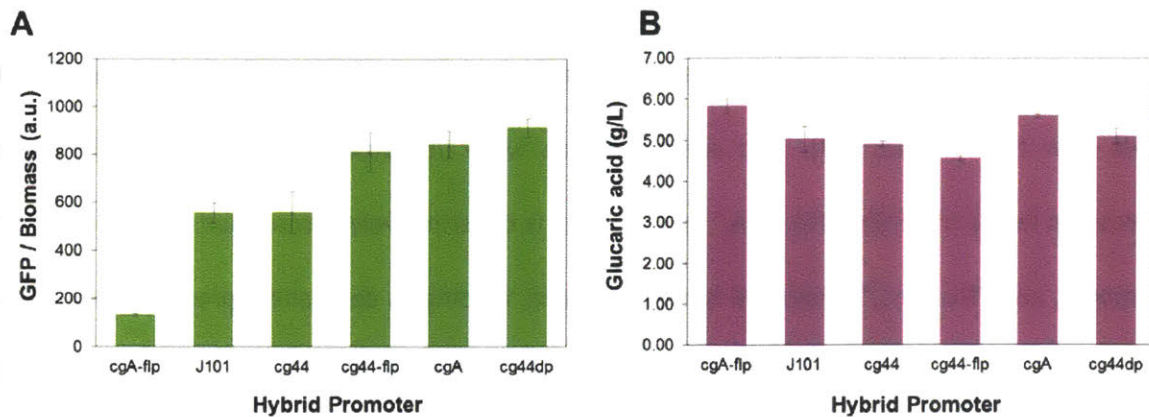
Figure 3.4. Relative fluorescence and glucaric acid production from different hybrid promoters. (A) GFP fluorescence from hybrid promoter variants (see Chapter 2, **Figure 2.2**) without ipsA expression, representing the maximum gfp expression levels. (B) Glucaric acid production from 10 g/L MI with MIOX driven by the corresponding hybrid promoters and udh integrated into the genome. J101 refers to the parent E. coli promoter (without any IpsA binding site) from which the hybrid promoters were derived. Error bars represent ± 1 S.D. from the mean of three replicate cultures.

To potentially optimize the dynamic control scheme and utilize the tunable MI biosensor, other hybrid promoter configurations (Chapter 2, **Figure 2.2**) were considered to drive expression of *Miox*. Different hybrid promoters led to varying maximum GFP levels of MI induction (**Figure 3.4**A), suggesting that higher maximum *Miox* transcription levels could be achieved. However, when the hybrid promoters were used to drive constitutive expression of *Miox* (without any dynamic regulation), no differences in glucaric acid production were observed (**Figure 3.4**B). This could be due to MI transport restrictions or limitations in translating and properly folding MIOX. Thus, we proceeded with the original selected hybrid promoter, cg44.

Although we found improved growth with IpsA present when only *INO1* was expressed (**Figure 3.5**), it is unlikely that the improvement in glucaric acid titer is due to the boost in growth, as we

did not observe significant growth benefits with the full pathway (**Figure 3.6**). As a control, we tested glucaric acid production with a circuit variant in which the promoter driving *Miox* did not contain an IpsA binding site (but is otherwise identical to the hybrid promoter) and observed no benefit in titer or growth (**Figure 3.7**). This indicates that the improvements in production from the biosensor circuit are not simply due to expression of *ipsA* or other circuit components.
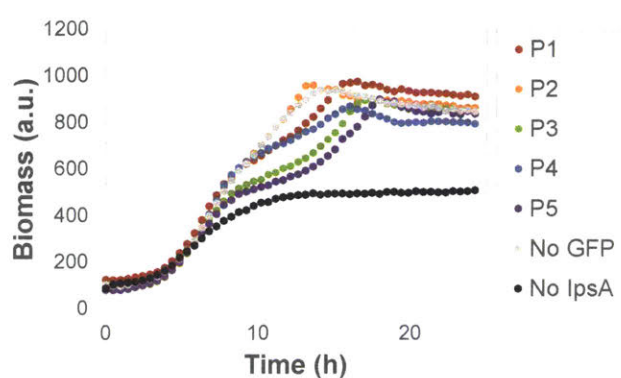
Figure 3.5. Growth curves for MG1655 (DE3) cells expressing the sensor circuit and *INO1*. Growth measured in BioLector biomass units (a.u.). The GFP negative control using the parent plasmid for the sensor (denoted "No IpsA") demonstrated poor growth compared to strains with promoters P1-P5 driving *ipsA*. A GFP negative control with *ipsA* expressed from P2 (denoted "No GFP") demonstrated comparable growth curves to strains with promoters P1-P5, suggesting that expression of *ipsA* leads to a boost in growth when *INO1* is simultaneously expressed from a separate plasmid. The boost in growth was not observed in strains expressing all three heterologous glucaric acid pathway enzymes (**Figure 3.6**). Values represent the mean of three replicate cultures.
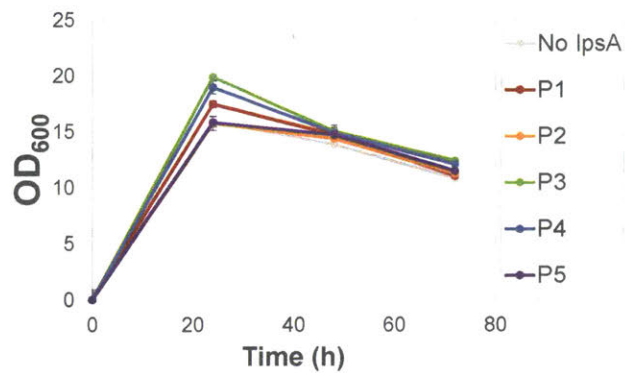
Figure 3.6. Optical density time course for glucaric acid production strains. Measurements taken 24, 48, and 72 hours post inoculation for MG1655 (DE3) $\Delta uxaC$ $\Delta gudD$ cells harboring plasmids encoding the glucaric acid pathway genes with *Miox* regulated by IpsA. Cells were cultured in T12 medium with 10 g/L glucose. Corresponding MI and glucaric acid titers are shown in **Figure 3.1**. Error bars denote ± 1 S.D. from the mean of three replicate cultures.
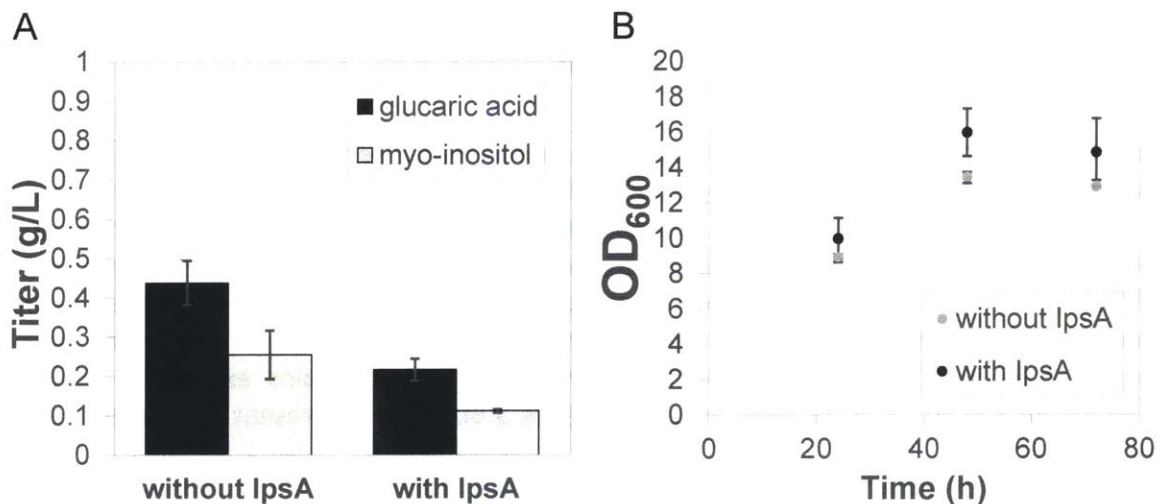
Figure 3.7. Glucaric acid production without MIOX control in the presence and absence of IpsA. (A) Glucaric acid and MI titer (g/L) and (B) optical density (OD_{600}) in the presence and absence of IpsA. MG1655(DE3) $\Delta uxaC$ $\Delta gudD$ harboring plasmids encoding the glucaric acid pathway genes with and without IpsA were cultured in T12 medium with 10 g/L glucose. For the strain without IpsA, IpsA-mediated regulation of *Miox* was removed by using the parent promoter to drive constitutive expression of *Miox*. Error bars denote ± 1 S.D. from the mean of three replicate cultures.

3.3.2   Layered Dynamic Regulation to Substantially Increase Production

While product titers were improved by instituting the MI biosensor strategy independently, we sought to implement even more precise regulation of the glucaric acid pathway by layering the QS-based Pfk-1 control system on top of the IpsA-based MI biosensor in the same strain (**Figure 3.8**). The QS-based system autonomously downregulates Pfk-1 at intermediate points in the fermentation to siphon carbon flux from glycolytic pathways to the glucaric acid pathway, while the IpsA-based MI biosensor delays transcription of *Miox* until threshold concentrations of MI have accumulated. Thus, we combined two tunable, orthogonal control systems, a pathway-independent and a pathway-dependent system, to synergistically boost pathway productivity. When acting independently in different strains, each system improved glucaric acid titers by 2 to 3-fold [63], suggesting that the combination of multiple pathway controls could boost titers even higher than either system alone.

The QS-based Pfk-1 control system was previously developed in our lab to institute autonomous, dynamic control at the G6P branch point, where carbon flux is split between native metabolic pathways and the heterologous glucaric acid production pathway. Upon buildup of the cognate N-acyl homoserine lactone (AHL), the circuit is triggered and leads to downregulation of Pfk-1, thereby limiting flux through glycolysis. The carbon flux is therefore redirected through MIPS into glucaric acid production. Expression of Pfk-1 is controlled by the P_{esaS} promoter, which is active in the absence of AHL. Upon AHL buildup, the promoter is deactivated, and transcription of its downstream gene is arrested. The triggering time can be tuned by modulating the AHL production rate by varying the expression of the AHL synthase, EsaI. A variety of expression rates

were obtained by instituting a library of promoter and ribosome binding site (RBS) variants

upstream of *esaI*. Stronger *esaI* expression leads to a higher AHL production rate and a faster

downregulation of Pfk-1 activity [63]. All circuit parts were genomically integrated, leading to a

series of strains, each with a distinct promoter-RBS combination driving *esaI* expression (L31GA,

L19GA, L24GA; **Table 3.3**). Similarly, timing of *Miox* expression was tunable in the MI biosensor

circuit through the varied expression levels of IpsA.
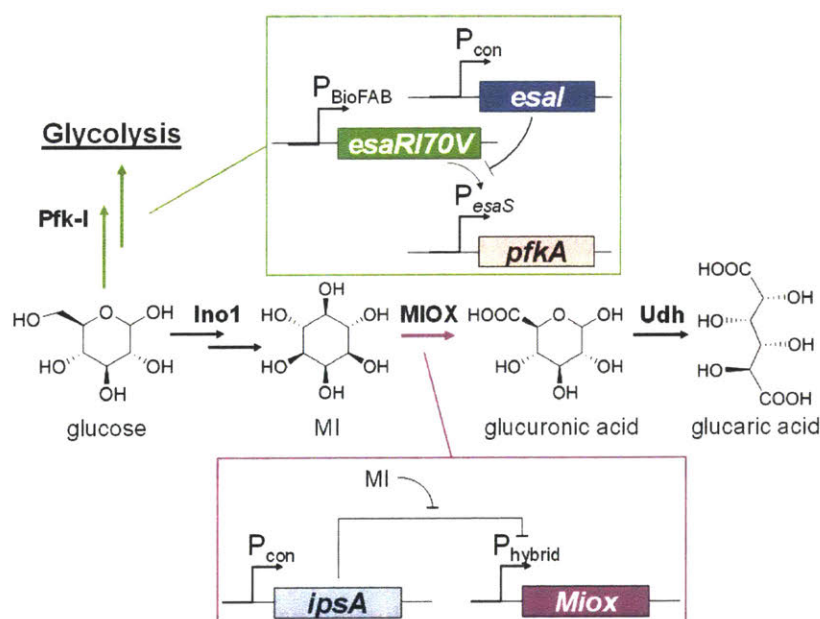
Figure 3.8. Schematic of layered dynamic regulation in the glucaric acid pathway. The initial branch point at glucose-6-phosphate (G6P) is controlled using a quorum sensing system, where *pfkA* placed under control of the P_{esaS} promoter is responsive to the AHL (produced by EsaI) concentration, corresponding to the cell density. Pfk-1 activity is knocked down at sufficiently high cell densities. Different levels of *esaI* expression, achieved by varying the strength of constitutive promoter P_{con}, alters the timing of *pfkA* knockdown. *Miox* is controlled via the cg44 hybrid promoter (Chapter 2, **Figure 2.1**) regulated by the MI-specific sensor IpsA.

In order to identify the optimal combination of Pfk-1 knockdown and *Miox* expression timing when both devices are present in the same strain, we tested each Esal expression level with each IpsA expression level. Strains contained *uxaC*, *gudD*, *zwf*, and *pfkB* knockouts to prevent product consumption and removal of carbon flux through other pathways (**Table 3.3**). At the 250-mL shake flask scale, strain "L19GA + P2" produced 1.84 g/L glucaric acid, the highest titer reported thus far in the *E. coli* K-12 strains. This is a 4.3 ± 0.051 fold increase in titer over the best-performing quorum sensing strain without *Miox* regulation, "L19GA + No IpsA," which produced 0.43 g/L glucaric acid, and a 9.1 ± 0.69 fold increase over the completely static strain "IB1379GA + No IpsA" (no *pfkA* knockdown or *Miox* delay), which produced only 0.20 g/L glucaric acid (**Figure 3.9**A and **Table 3.4**). In our previous work, strain L19GA (without IpsA) produced 0.68 g/L glucaric acid[63], slightly more than strain "L19GA + No IpsA" in this work. However, different expression vectors for the pathway genes were used due to the need to accommodate and be consistent with the MIOX regulatory circuit developed in this work. These differences, perhaps including the additional expression of *ipsA*, are the most likely causes of the discrepancy in titers. Generally, we found that intermediate Pfk-1 knockdown times, along with intermediate *Miox* expression times, led to improved titers. To ensure that IpsA itself did not render growth and production benefits, we also expressed *ipsA* with *Miox* driven by a promoter that was not regulated by IpsA, and observed no boost in titer over the control strain not expressing *ipsA* (**Figure 3.10**). Strain "L19GA + P2" was chosen for scale-up in a 3-L bioreactor with dissolved oxygen and pH control. This strain produced 1.98 g/L glucaric acid, corresponding to 20% yield by mass, while strain "L19GA + No IpsA" only produced 0.4 g/L glucaric acid (**Figure 3.9**B).

Table 3.4. Glucaric acid (GA) and *myo*-inositol (MI) titer for layered regulation strains (**Table 3.3**). Final titers measured after 72 hours fermentation in T12 with 10 g/L glucose. Values reported as described in the table legend.

	No IpsA			P1			P2		
IB1379GA	0.20 ± 0.00	0.14 ± 0.01		0.58 ± 0.01	0.33 ± 0.02		0.65 ± 0.02	0.29 ± 0.01	
	0.96 ± 0.01	0.75 ± 0.06	1.71	2.77 ± 0.06	1.83 ± 0.09	4.60	3.10 ± 0.08	1.63 ± 0.07	4.73
L31GA	0.59 ± 0.02	0.19 ± 0.02		0.79 ± 0.02	0.24 ± 0.00		0.64 ± 0.03	0.57 ± 0.03	
	2.82 ± 0.10	1.07 ± 0.11	3.89	3.75 ± 0.09	1.35 ± 0.02	2.96	3.04 ± 0.16	3.19 ± 0.17	4.62
L19GA	0.43 ± 0.04	0.35 ± 0.03		0.63 ± 0.02	0.19 ± 0.00		1.84 ± 0.14	0.32 ± 0.04	
	2.03 ± 0.18	1.96 ± 0.17	3.99	2.99 ± 0.11	1.07 ± 0.02	4.06	8.75 ± 0.65	1.79 ± 0.20	10.54
L24GA	0.00 ± 0.00	0.16 ± 0.01		0.45 ± 0.05	0.15 ± 0.01		0.74 ± 0.05	0.20 ± 0.01	
	0.00 ± 0.00	0.90 ± 0.07	4.77	2.13 ± 0.23	0.84 ± 0.04	5.09	3.52 ± 0.22	1.10 ± 0.05	6.23

	P3			P4			P5		
IB1379GA	0.53 ± 0.05	0.26 ± 0.02		0.29 ± 0.01	0.29 ± 0.01		0.27 ± 0.01	0.23 ± 0.01	
	2.51 ± 0.23	1.44 ± 0.11	3.95	1.40 ± 0.03	1.61 ± 0.03	3.01	1.28 ± 0.04	1.26 ± 0.03	2.54
L31GA	0.63 ± 0.03	0.49 ± 0.02		0.19 ± 0.00	0.12 ± 0.01		0.64 ± 0.08	0.20 ± 0.01	
	3.01 ± 0.15	2.74 ± 0.08	5.75	0.91 ± 0.02	0.68 ± 0.03	3.76	3.05 ± 0.36	1.11 ± 0.06	2.13
L19GA	1.69 ± 0.04	0.45 ± 0.01		0.44 ± 0.03	0.22 ± 0.02		0.17 ± 0.01	0.14 ± 0.00	
	8.03 ± 0.17	2.49 ± 0.04	10.52	2.10 ± 0.14	1.21 ± 0.09	3.30	0.79 ± 0.03	0.76 ± 0.00	1.55
L24GA	0.33 ± 0.01	0.18 ± 0.01		0.36 ± 0.02	0.37 ± 0.01		0.24 ± 0.03	0.18 ± 0.01	
	1.56 ± 0.03	1.02 ± 0.03	0.91	1.69 ± 0.08	2.07 ± 0.06	1.59	1.13 ± 0.16	0.99 ± 0.03	4.16

Table Legend.

	Promoter Driving *ipsA*		
Strain Name	GA (g/L) ± 1 S.D.	MI (g/L) ± 1 S.D.	
	GA (mM) ± 1 S.D.	MI (mM) ± 1 S.D.	Sum of GA+MI (mM)
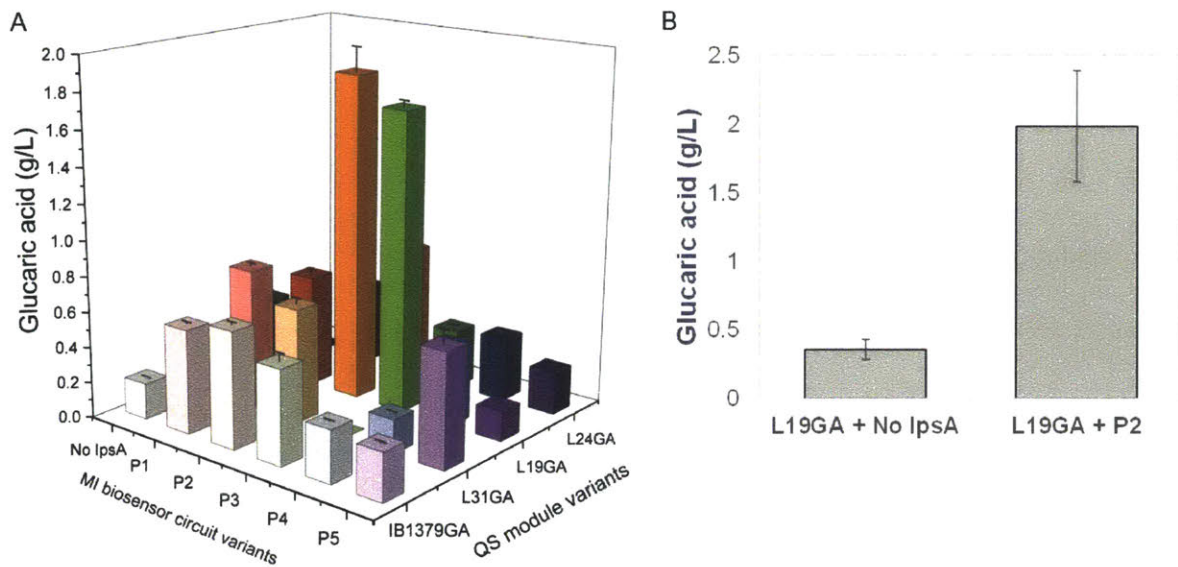
Figure 3.9. Glucaric acid production from strains with layered dynamic regulation at 72 hours. (A) Glucaric acid titer as a function of Pfk-1 switching time (QS module variants) and *Miox* expression time (MI biosensor circuit variants) at the 250-mL shake flask scale. Error bars represent ± 1 S.D. from the mean of three replicate flasks. (B) Glucaric acid production at the 3-L bioreactor scale for strains L19GA + P2 and L19GA + No IpsA. Error bars represent ± 1 S.D. from the mean of two replicates. No IpsA: constitutive (unregulated) *Miox* expression. IB1379GA: wild-type *pfkA* expression (no knockdown of *pfkA*).

The combination of the two orthogonal regulation strategies in one pathway demonstrates synergistic effects, as the titer from the composite strain was greater than when either strategy was evaluated alone. The Pfk-1 switch shunts flux towards MIPS and away from glycolysis, improving MI production. Addition of the second layer expresses *Miox* at an optimal time, further boosting titers. The use of orthogonal, tunable controllers allowed the identification of optimal switching times for each independent device. While many combinations of MIOX and Pfk-1 regulation systems showed improved production over the completely static, unregulated strain "IB1379GA + No IpsA" (**Figure 3.9**A), only two strains produced over 1.5 g/L glucaric acid, demonstrating that tuning is required for optimization. For the *pfkA* downregulation switch,

strain "L19GA" was the highest-producing strain for both single dynamic regulation[63] and layered regulation. However, the optimal *Miox* expression switch varied by strain background: promoter P4 for the single regulation system, and P2 for the layered regulation system. As *pfkA* downregulation affects MI production and therefore the timing and dynamics of *Miox* expression, the MIOX control switch is more sensitive to differences in strain background. In the layered control system, *pfkA* and *Miox* are expressed only when necessary, as we move closer towards the concept of "just-in-time" transcription[51] in heterologous pathways, a widespread phenomenon that exists in native pathways such as amino acid biosynthesis[51,98], arabinose utilization[99], and metal resistance mechanisms[39].
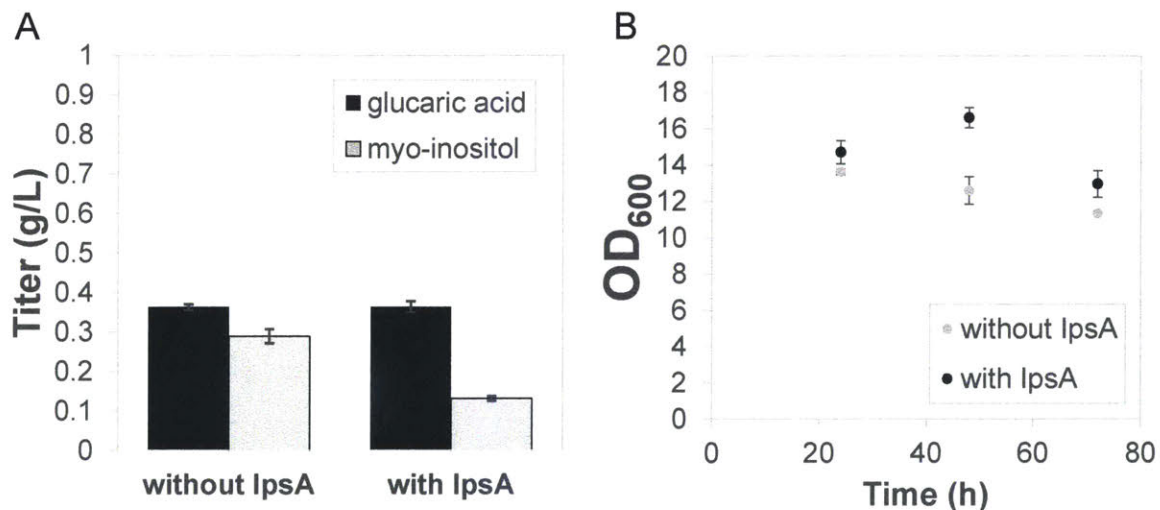
Figure 3.10. Glucaric acid production without MIOX control in the presence and absence of IpsA. (A) Glucaric acid and MI titer (g/L) and (B) optical density (OD_{600}) in the presence and absence of IpsA. Strain L19GA harboring plasmids encoding the glucaric acid pathway genes with and without IpsA were cultured in T12 medium with 10 g/L glucose. For the strain without IpsA, IpsA-mediated regulation of *Miox* was removed as in **Figure 3.7**. Error bars denote ± 1 S.D. from the mean of three replicate cultures.

3.3.3 Alternate Regulation Designs

The "simple regulation" approach described above was successful in improving glucaric acid production, but more complex modes of regulation might further optimize the system. Two alternative types of regulation were investigated: auto-regulation and the toggle switch.
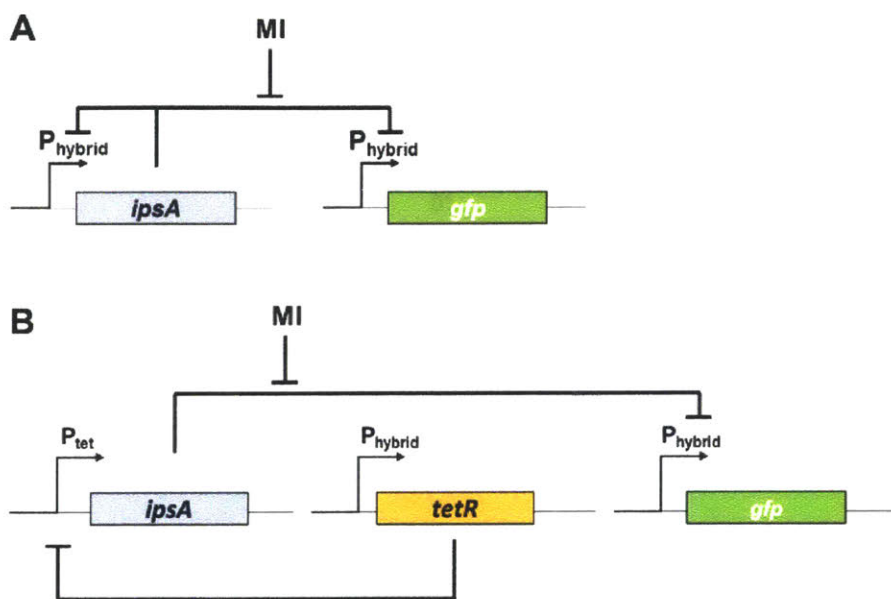
Figure 3.11. Schematic of circuit design for alternative modes of dynamic regulation. (A) Auto-regulated IpsA, where IpsA represses itself as well as the reporter *gfp*. (B) Toggle switch, where TetR represses *ipsA*, and IpsA represses *tetR* as well as the reporter *gfp*.

3.3.3.1 Auto-regulation

Many biological systems are auto-regulated to allow a faster response to changes in the environment[100]. IpsA is natively auto-regulated in *C. glutamicum*[85]. To implement auto-regulation, the IpsA binding site cgA (see Chapter 2) was placed in the promoter driving expression of *ipsA*, leading IpsA to repress its own transcription (**Figure 3.11**A). We observed that addition of the

binding sequence to the promoter altered the dose response curve profiles (**Figure 3.12**), the

relative promoter strengths, and leakiness (**Figure 3.13**).
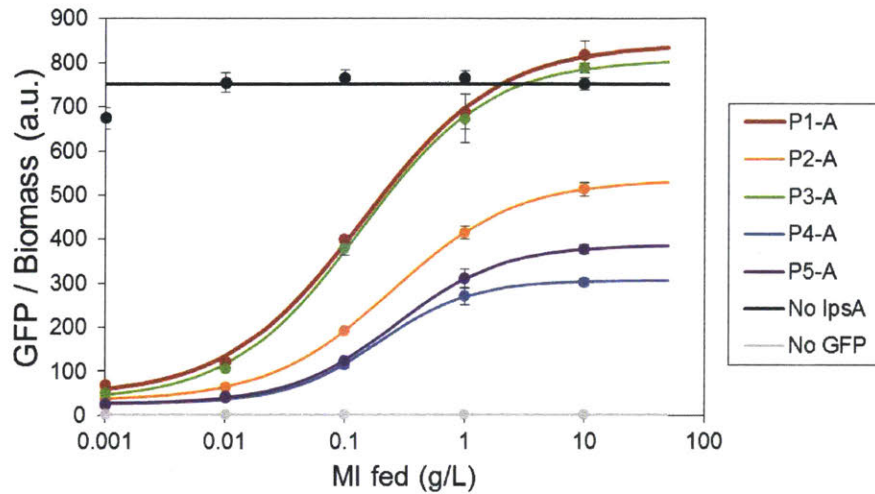
Figure 3.12. Dose response curves for auto-regulated IpsA. Cells harboring the auto-regulated biosensor system (self-repressing IpsA) were fed MI at inoculation. GFP measurements taken at 24 h. Error bars represent ±1 S.D. from the mean of three replicate cultures.
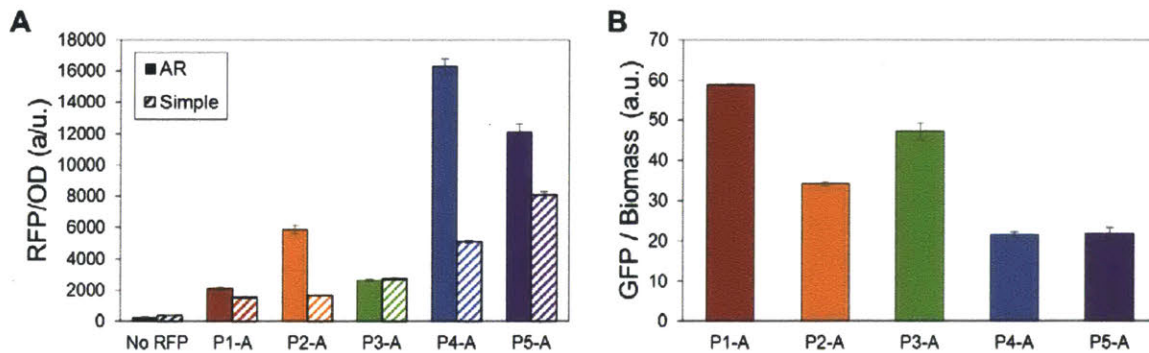
Figure 3.13. Characteristics of auto-regulated promoters. (A) Relative promoter strengths as measured by RFP. AR refers to promoters containing the cgA binding sequence. Simple refers to promoters without the auto-regulatory sequence, the same promoters as Figure 2.3. (B) Leakage levels of AR promoters as measured by GFP at 0 g/L MI.

However, initial characterization of this system with cells producing MI from MIPS did not result in a faster response in GFP fluorescence than the simple regulation system (**Figure 3.14**), nor did it improve glucaric acid production when applied to the full pathway (data not shown). Addition of the cgA binding sequence generally increased the promoter strength as measured by RFP fluorescence (**Figure 3.13**A). This would increase the amount of IpsA in the cell as compared to the simple regulation system, which might have negated any auto-regulation effect. Furthermore, the auto-regulation system implemented had two separate binding sites, and the distribution of IpsA molecules between the two sites could affect the GFP response. Because auto-regulation did not improve glucaric acid production, this dynamic regulation mode was not further explored.
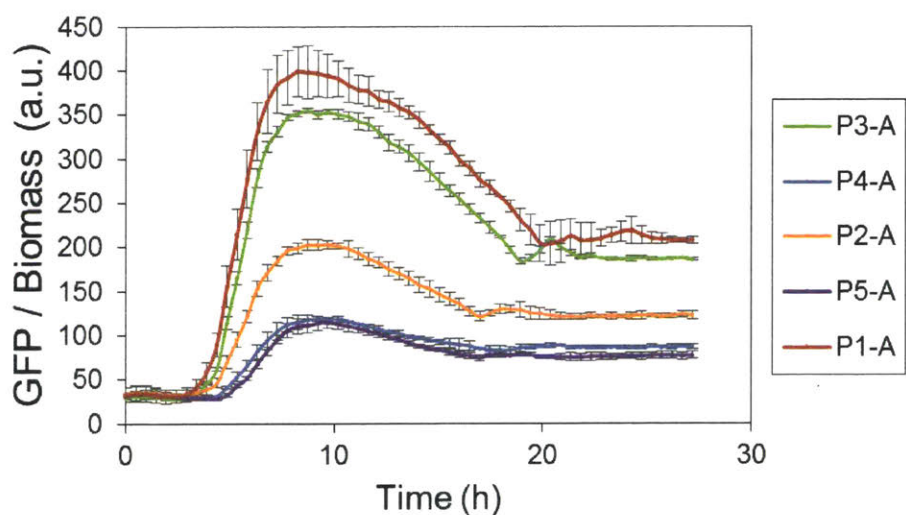
Figure 3.14. GFP time course of auto-regulated biosensor with cells producing MI. MG1655 (DE3) produced MI from endogenous phosphatase and over-expression of *INO1*. P1-A through P5-A denote the auto-regulated promoters, altered from P1-P5 promoters in **Figure 2.5**. Error bars represent ± 1 S.D. from the mean of three replicate cultures.

3.3.3.2 Toggle Switch

The toggle switch is a regulation system that permits an effectively permanent switch from one stable state to another[101]. This system was explored in the context of the glucaric acid pathway because it would allow MIOX transcription to remain "on" even as MIOX consumed MI. To design the toggle switch, we used a dual-repressor system, where TetR repressed *ipsA* driven by the Ptet promoter, and IpsA in turn repressed *tetR*, driven by the hybrid promoter containing the IpsA binding site (**Figure 3.11**B). IpsA also repressed the hybrid promoter driving the GFP fluorescent reporter for toggle switch characterization. While we attempted to tune the promoter and RBS strengths for each of the repressor genes, we were unable to achieve bistability, a phenomenon where GFP would remain stably "on" after MI was removed from the medium. This might be because bistable networks require at least one of the repressor systems to be very cooperative[101]. Further troubleshooting would involve using LacI as the second repressor instead of TetR, as LacI is a known cooperative system, and all successful reported toggle switches have used LacI as one of the repressors[96,101,102].

3.4 Conclusions

Dynamic regulation is a metabolic engineering strategy for improving production in pathways with toxic intermediates, essential competing reactions, or flux imbalances. The layered dynamic control system employed here mimicked natural regulatory systems by upregulating a downstream enzyme only upon sufficient production of its intermediate, and downregulating an essential competing enzyme upon sufficient cell growth. The combinatorial search through the two systems suggests that the timing of induction and repression must be carefully tuned to identify the optimal producer. More complex modes of regulation were also explored but did not lead to expected dynamic behavior or improved production. This work demonstrates the potential of using multiple, independently-controlled regulation strategies to implement process control at the cellular level.

4. Directed Evolution of MIPS

Abstract

Myo-inositol (MI), a component of cell membranes and a signaling molecule in the brain, is a dietary supplement and a precursor to biologically active compounds and renewable chemicals. MI has been produced in *E. coli* by heterologous expression of *S. cerevisiae INO1*, encoding *myo*-inositol-phosphate-synthase (MIPS), which catalyzes the reaction from glucose-6-phosphate to *myo*-inositol-1-phosphate. Engineering MIPS using directed evolution is one strategy to improve MI production, but the testing of large mutagenesis libraries is limited by screening throughput. Here we use a MI biosensor, which couples MI production to GFP fluorescence, as a high-throughput screen to identify improved MIPS mutants generated by error-prone PCR. The screen identified mutants producing up to a 20% increase in MI titers. This approach demonstrates the value of the biosensor as high-throughput screening tool, which enables the use of powerful protein engineering methods in pathway improvement.

4.1 Introduction

Myo-inositol (MI) is a six-carbon sugar commonly used in the food and chemical industries. MI is a dietary supplement, an additive in animal feeds[103], an intermediate to D-glucaric acid – a component of detergents and nylons[75], and a precursor to a variety of biologically active compounds including 1,2,3,4-tetrahydroxybenzene and the antioxidant coenzyme Q[104]. In native contexts, MI is a precursor to phospholipids in cell membranes and an important signaling molecule in the brain[105]. Conventional MI production occurs by hydrolysis of phytic acid extracted from seeds, which requires an initial separation process, high temperatures and pressures, and acidic conditions[106]. A more environmentally-friendly MI production process from glucose in *E. coli* has been demonstrated by over-expressing *myo*-inositol-phosphate-synthase (EC 5.5.1.4; MIPS) from *S. cerevisiae*, achieving 11% yield[104,107]. MIPS is a highly conserved enzyme that catalyzes the reaction from glucose-6-phosphate (G6P) to *myo*-inositol-1-phosphate (M1P), and is the rate-limiting first step in all inositol biosynthesis pathways[108,109].

In *E. coli*, MIPS faces steep competition with central carbon metabolism, and there have been efforts to make the G6P to M1P conversion more favorable. Most strategies have focused on dynamic knockdown of glycolysis to separate biomass formation from production. During the production phase, glycolytic enzymes are degraded and not expressed, increasing the G6P pools available for MIPS[62,63]. Other strategies bypass cell growth altogether by employing *in vitro* enzymatic conversions of starch to MI[106,110].

Protein engineering to improve the MIPS enzyme itself has not been extensively explored. Despite crystal structures available for a few MIPS homologs, including *S. cerevisiae* MIPS[111], highly conserved motifs and catalytic residues are scattered across the enzyme, making the active site difficult to rationally re-design[112]. The homo-tetrameric enzyme also requires the co-factor NAD+, which is regenerated during the course of the reaction[111,113], but the co-factor binding pocket adds complexity in terms of rational protein design.

Directed evolution is a powerful protein engineering strategy to engineer improved enzymes[66]. Because most mutants generated by random mutagenesis techniques are neutral or deleterious, large libraries are necessary for identifying desired mutants, and screening is often the rate limiting step in the evolution process[23,26]. One high-throughput screening tool is a genetically encoded, whole cell biosensor. In a biosensor-based screen, the cell acts as its own analytical device by detecting the reaction product and relaying the signal through a phenotypic reporter such as GFP. These detection systems are derived from natural regulation mechanisms such as transcription factors and riboswitches, and their signals are re-wired to output a visible or selectable marker. Many biosensors have been identified and engineered to detect numerous compounds including amino acids[40], metals[114], and CoA building blocks[57,59].

Biosensors have been used as high-throughput screens in mutagenesis libraries to improve enzyme activities and in metagenomic libraries to identify novel protein functions[70]. A lysine-responsive transcription factor in *C. glutamicum* was used to screen a directed evolution library

of pyruvate carboxylate, the enzyme responsible for replenishing the TCA intermediates required for amino acid biosynthesis[72]. A similar biosensor that detected arginine was used to screen a library of N-acetyl-L-glutamate kinases, identifying mutants that relieved allosteric arginine inhibition of the enzyme by 20-fold[40]. A transcription factor engineered to recognize ectoine was applied as a high-throughput screen for mutant diaminobutyrate-2-oxoglutarate (DABA) aminotransferases, the rate-limiting step in ectoine biosynthesis, thereby improving heterologous ectoine production in *E. coli*[49]. Similarly, an engineered triacetic acid lactone biosensor identified a 2-pyrone synthase mutant with 19-fold increase in catalytic efficiency[48]. In these cases, combining directed evolution strategies with high-throughput screening capabilities of biosensors enabled significant pathway improvements.

Here we use a genetically encoded MI biosensor to screen libraries of MIPS variants in order to identify improved MI producers. The best-performing mutant V251I produced 20% more MI than the wild-type yeast MIPS.

4.2 Materials and Methods

4.2.1 Sensor and Library Construction

All primers used in this study are found in **Table 4.1**. All plasmids used in this study are found in

Table 4.2. Unless otherwise specified, all enzymes were purchased from New England Biolabs

(Ipswich, MA).

To allow compatibility with the vector expressing MIPS, the antibiotic selection marker on the

MI biosensor plasmid (Chapter 2) was changed from kanamycin to streptomycin by CPEC[89] using

primers pHH-Strep-F, pHH-Strep-R, Strep-pHH-F, and Strep-pHH-R. The catalytically inactive

version of MIPS, pRSFD-MIPS(K489A), was generated using primers IN-K489A-F and IN-K489A-R

with the Site-Directed Mutagenesis Kit (New England Biolabs, Ipswich, MA) following

manufacturer instructions.

Selected mutants (**Figure 4.6**A) were cloned into a fresh background strain by mini-prepping the

plasmids from isolated colonies and digesting the plasmids with EcoRI and HindIII to yield the

mutant MIPS fragment. The fragment was then ligated into the digested vector backbone. Single

amino acid mutants (without silent mutations) were constructed by the Site-Directed

Mutagenesis Kit using primers X#Y-F and X#Y-R, where X refers to the original residue, # refers to

the residue position in the primary sequence, and Y refers to the mutated residue.

MIPS libraries were generated by error-prone PCR (epPCR) with primers IN-Lib-F and IN-Lib-R

using GeneMorph II Random Mutagenesis Kit (Agilent Technologies, Santa Clara, CA) following

manufacturer instructions. For the test library, the epPCR product was purified by gel

electrophoresis, digested with high-fidelity restriction enzymes EcoRI and HindIII, and ligated into

the backbone. To prepare the backbone, the vector pRSFD-MIPS(K489A) was digested with the

same restriction enzymes and de-phosphorylated with rSAP. The inactive version of MIPS was

used as a stuffer fragment to decrease background levels in the final library. For the full-sized

libraries, truncated mutants were removed by gel purification of full sized product after the

epPCR product was digested. Mutation rate was controlled by amount of template addition.

Following the epPCR, DpnI was added to the reaction to remove template plasmid. The product

was subsequently digested, purified by gel electrophoresis, and ligated into backbone. Ligation

products were used to transform NEB-5α high competent cells (New England Biolabs, Ipswich,

MA). After 24 h growth at 30°C, the colonies were pooled in LB and mini-prepped to isolate the

plasmid library. The plasmid library was then used to transform MG1655 (DE3) or BL21 (DE3) cells

harboring sensor plasmid pSNR2-cg44dp-GFP-P5-ipsA (Chapter 2). For the test library, MG1655

(DE3) was used. For subsequent libraries, BL21 (DE3) was used. At this stage, 8-10 colonies were

randomly selected to estimate the mutation rate and library diversity. The final library was

pooled in LB and stored in at a final concentration of 15% w/v glycerol at -80°C.

Table 4.1. List of primers used in this study.

Name	Sequence
pHH-Strep-F	caggatgaggatcgtttcgcatgagggaagcggtgatcgc
pHH-Strep-R	gaataggaacttcaagatccccttatttgccgactaccttggtgatctc
Strep-pHH-F	gcgatcaccgcttccctcatgcgaaacgatcctcatcctg
Strep-pHH-R	gagatcaccaaggtagtcggcaaataaggggatcttgaagttcctattc
IN-K489A-F	cgctccattaacaagaccagg
IN-K489A-R	gctaaccagtaactcaagaagg
IN-Lib-F	cacagccaggatccgaattc
IN-Lib-R	ttatgcggccgcaagcttcta
Y250S-F	cgtagaagtatctcctggtg
Y250S-R	gacctctcagtatttgcagtcc
S79T-F	ccactttagtggcctcggtattg
S79T-R	tgccattgttgccacctaac
V251I-F	tagaagtatctcctggtgttaatg
V251I-R	tgtacctctcagtatttgcagtc
I377T-F	agatgacatcatcgcgtctaatg
I377T-R	gtgacagaacttttggaaatctcc

Table 4.2. List of plasmids used in this study.

Plasmid	Description	Reference
pSNR2-cg44dp-GFP-P5-ipsA	Sensor plasmid, contains MI-responsive transcriptional regulator IpsA, which regulated GFP	Chapter 2
pRSFD-IN	pRSFDuet with wild-type *S. cerevisiae* MIPS	[77]
pRSFD-MIPS(K489A)	pRSFDuet with catalytically inactive *S. cerevisiae* MIPS	This study
pRSFD-MIPS(Y250S)	*S. cerevisiae* MIPS with Y250S mutation	This study
pRSFD-MIPS(L321F)	*S. cerevisiae* MIPS with L321F mutation	This study
pRSFD-MIPS(S79T)	*S. cerevisiae* MIPS with S79T mutation	This study
pRSFD-MIPS(V251I)	*S. cerevisiae* MIPS with V251I mutation	This study
pRSFD-MIPS(I377T)	*S. cerevisiae* MIPS with I377T mutation	This study
pRSFD-MIPS(V251I / I377T)	*S. cerevisiae* MIPS with V251I and I377T mutations	This study
pRSFD-His-INO1	*S. cerevisiae* MIPS with N-terminal His tag	This study
pRSFD-INO1-opt	*S. cerevisiae* MIPS, codon optimized for *E. coli*	Prather lab
pRSFD-His-INO1-opt	*S. cerevisiae* MIPS, codon optimized with His tag	This study
pTrc-INO1	*S. cerevisiae* MIPS on pTrc99A vector	[77]
pTrc-His-INO1	*S. cerevisiae* MIPS with N-terminal His tag	This study
pTrc-INO1-opt	*S. cerevisiae* MIPS, codon optimized for *E. coli*	Prather lab
pTrc-His-INO1-opt	*S. cerevisiae* MIPS, codon optimized with His tag	This study

4.2.2 Flow Cytometry and Cell Sorting

For flow cytometry analysis, cells were diluted in phosphate buffered saline (PBS) and analyzed on FACSCanto II (BD Biosciences, Franklin Lakes, NJ) with a 488 nm laser and a 530/30 band-pass filter. Populations were gated on forward and side scatter to remove analysis of events containing debris and doublets.

For sorting MIPS libraries, one 600 μL glycerol stock aliquot was thawed into a 250-mL baffled shake flask containing 30 mL LB (Luria-Bertani broth) with 6 g/L glucose, appropriate antibiotics, and 100 μM isopropyl β-D-1-thiogalactopyranoside (IPTG). The library was cultured for approximately 18 h at 30°C, 250 rpm, and 80% humidity. Cells were then washed with PBS + 1% w/v sucrose by centrifuging 5 min, 3000 x g, and re-suspended in PBS + 1% w/v sucrose. Washed cells were immediately sorted with FACSAria III (BD Biosciences, Franklin Lakes, NJ) with a 488 nm laser and a 530/30 band-pass filter. The top 0.5-1% GFP positive population (after gating on forward and side scatter to exclude debris and doublets) was collected. Cells were collected in 1 mL LB, recovered for 30 minutes shaking at 37°C, and expanded to a 5 mL overnight outgrowth culture with antibiotic selection at 30°C. Recovered cultures were plated on LB agar with appropriate antibiotics to yield single colonies for testing and stored in glycerol at -80°C for subsequent rounds of sorting.

4.2.3   Fermentation

Fermentation cultures were inoculated from overnight cultures in LB with appropriate antibiotics at a dilution of 1:100 vol/vol. Fermentation was carried out for 3 days in the BioLector (m2p labs, Baesweiler, Germany). Cultures were grown in flower plates (m2p labs) containing 1 mL medium per well, 30°C, 1200 rpm, 80% humidity. The medium contained LB with 6 g/L glucose, appropriate antibiotics, and 100 uM IPTG. Biomass (backscattered light at 620 nm) and GFP (488 nm excitation / 520 nm emission) measurements were taken by the BioLector every ~15 min.

4.2.4   Product Quantification

Culture supernatants were sampled for glucose and MI quantification. Samples were measured by high performance liquid chromatography on an Agilent 1200 series instrument (Agilent, San Jose, CA) with an Aminex HPX-87H column (Bio-Rad, Hercules, CA) maintained at 45°C and refractive index detector (RID) at 35°C. Samples were run on a 22 minute, isocratic method with 5 mM sulfuric acid mobile phase at a flow rate of 0.6 mL / minute. Elution times for relevant species are MI at 9.5 minutes and glucose at 9.1 minutes.

4.3   Results and Discussion

A MI biosensor that outputs GFP in the presence of MI was previously constructed in our group based on the MI-responsive transcriptional regulator IpsA from *C. glutamicum* (Chapter 2 and **Figure 4.1**). The sensor was capable of detecting MI at levels produced by heterologous expression of MIPS. The sensor version with the highest dynamic range had a hybrid promoter with two cg44 operator sites, located upstream of the -35 and downstream of the -10 hexamers (**Figure 2.2**, Chapter 2). This sensor version had the desirable characteristics of low leakiness (baseline level of GFP) to easily distinguish producers from non-producers, and a high maximum level of GFP, such that increases in MI production above that of wild-type *S. cerevisiae* MIPS could be detected.
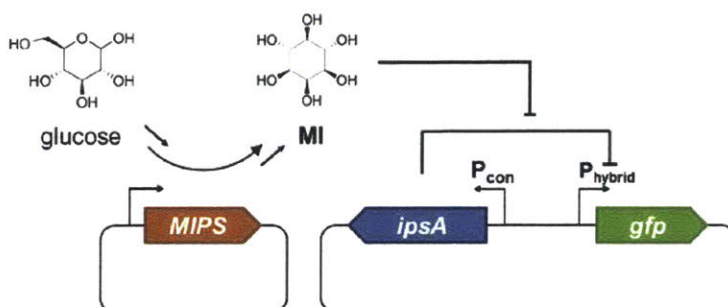
Figure 4.1. Schematic of biosensor and MIPS plasmids. MIPS, with the phosphotransferase (PTS) system and phosphatase convert glucose to MI, which induces *gfp* expression.

4.3.1   Biosensor Validation

To validate that the sensor could distinguish differences in MI production, the sensor was used to detect MI production from a set of MIPS homologs[84]. As a control, a catalytically inactive version of *S. cerevisiae* MIPS, MIPS(K489A), was constructed based on mutation studies from *A.*

fulgidis MIPS and a sequence alignment[115]. The trend in GFP measurements tracked that of MI titers (**Figure 4.2**), confirming utility of the MI biosensor for identifying better producers.
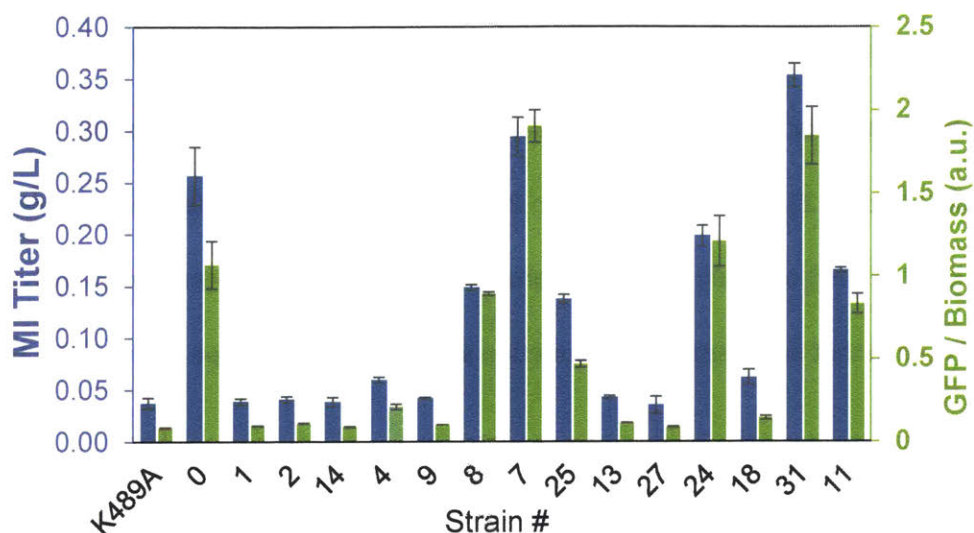
Figure 4.2. MI titer (blue) and GFP fluorescence (green) of different MIPS variants. Samples were taken 48 h post inoculation from cultures of BL21 (DE3) cells harboring the MIPS plasmid and sensor plasmid. Strain number refer to previously tested MIPS homologs[84]. K489A: catalytically inactive MIPS. 0: *S. cerevisiae* MIPS, the original variant used in the pathway. Error bars represent ± 1 S.D. from the mean of three biological replicates.

To determine which vector conditions would provide the optimal template for directed evolution, the MI biosensor was used to compare codon optimization, addition of an N-terminal His-tag, and expression vector. Production was compared with and without the biosensor to further validate sensor utility (**Figure 4.3**). While the pTrc vector appeared to be the best-performing, the GFP signal from the MI biosensor dropped between 24 and 48 h, likely due to acetate

production degrading the GFP. Thus we continued with pRSFDuet as the expression vector for MIPS.
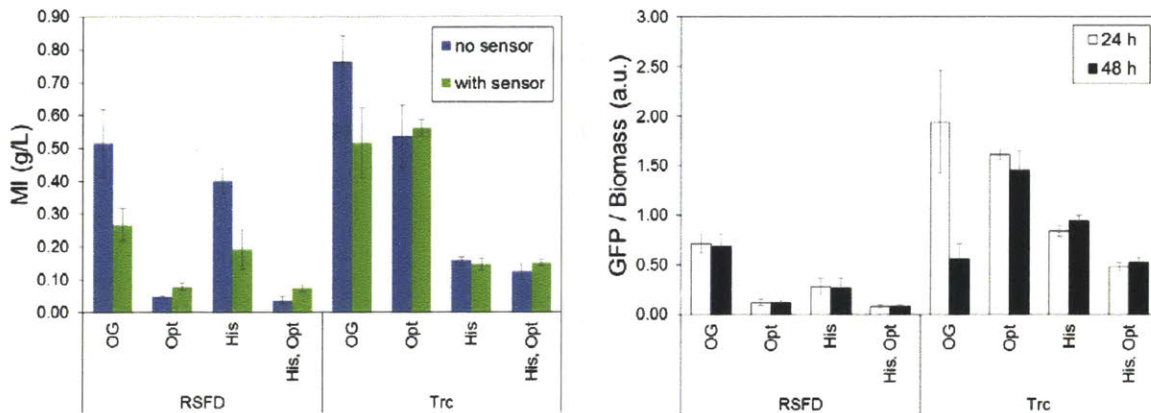
Figure 4.3. Comparison of MIPS vector conditions. (Left) MIPS expressed in BL21 (DE3) from pRSFDuet or pTrc vectors, with or without His tag (His), codon optimization (Opt), or the sensor plasmid. OG – original *S. cerevisiae* MIPS gene without any modifications. (Right) GFP values at 24 and 48 h of the strains harboring the sensor plasmid. Error bars represent ± 1 S.D. from the mean of three biological replicates.

Next, we ensured that the whole-cell biosensor could be used in a one-pot format for flow cytometry. A test sort was implemented to determine whether MI produced by functional MIPS diffused into cells with non-functional MIPS, leading to "cheaters" that are fluorescent but non-producing. A culture was inoculated in varying ratios of wild-type to catalytically inactive MIPS(K489A). After growth into stationary phase, the number of GFP positive cells was counted by flow cytometry. The number of GFP positive cells was lower than the expected amount based on inoculation ratios (**Figure 4.4**), possibly due to a selective advantage for non-GFP producers. However, the bi-modal distributions of GFP positive and GFP negative populations were

maintained, showing that MI diffusion was not significant enough to homogenize the entire population. To further confirm that the GFP positive cells were wild-type, cells with high fluorescence intensities were collected via fluorescence activated cell sorting (FACS). Collected cells were plated on selective medium to yield single colonies that were sequenced, resulting in 7 out of 8 wild-type MIPS (and 1 catalytically inactive MIPS). As no significant cheating was observed, we proceeded with the FACS method to identify better-producing MIPS mutants.
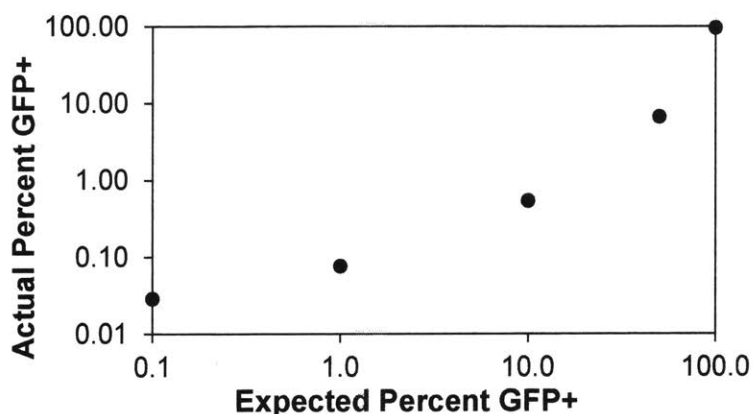
Figure 4.4. Proportion of GFP positive cells measured by flow cytometry. BL21 (DE3) cells harboring the sensor plasmid and either MIPS or MIPS(K4898A) were inoculated with varying ratios of wild-type to catalytically inactive MIPS. Expected percent GFP+ refers to the percentage of cells with wild-type, active MIPS at inoculation.

4.3.2 Library Generation and Sorting

Three mutant libraries were generated by error-prone PCR on the *S. cerevisiae* MIPS template. Initially, a ~3000-member test library with an average of 3 amino acid changes per gene and 20% truncations was constructed. The truncated genes conferred a selective growth advantage, and the subsequent library versions were constructed in a manner which removed the truncations

(see Methods). The subsequent libraries had roughly 1 million members. A high mutation rate library with an average of ~9 amino acid (~12 bp) changes per gene and a low mutation rate library with ~2 amino acid (~2 bp) changes per gene were constructed. While low mutation rates tend to preserve function, high mutation rates have been shown to allow access to more mutation diversity[116]. The libraries were subjected to multiple rounds of sorting, with the top 0.5-1% GFP positive cells collected at each sort, in order to enrich the population of high-fluorescent (and hopefully high-producing) cells. GFP population histograms for each library and sorting round are shown in **Figure 4.5**.

4.3.3   Hit Validation

Single colonies were isolated from each round and tested for improved MI production. Colonies were sequenced if final MI titers were higher than a cutoff value based on wild-type level titers (**Table 4.3** and **Table 4.4**). Wild-type titers varied considerably with each test, so the cutoff values were adjusted for each test. Because wild-type MIPS did not produce MI when testing isolated clones from low mutation rate library round 3, a cutoff of 0.3 g/L MI was used for that round. For high mutation rate library round 2, wild-type MIPS produced more MI than typically observed, which would have led to very few hits for further processing, so a more generous cutoff of 0.7 g/L MI was chosen. Many isolated clones were wild-type, likely because the library populations, even after enrichment, did not yield cells with fluorescence levels much brighter than wild-type (**Figure 4.5**). Many mutants appeared multiple times, suggesting that the enrichment process did bias the population toward a set of high-fluorescent clones.
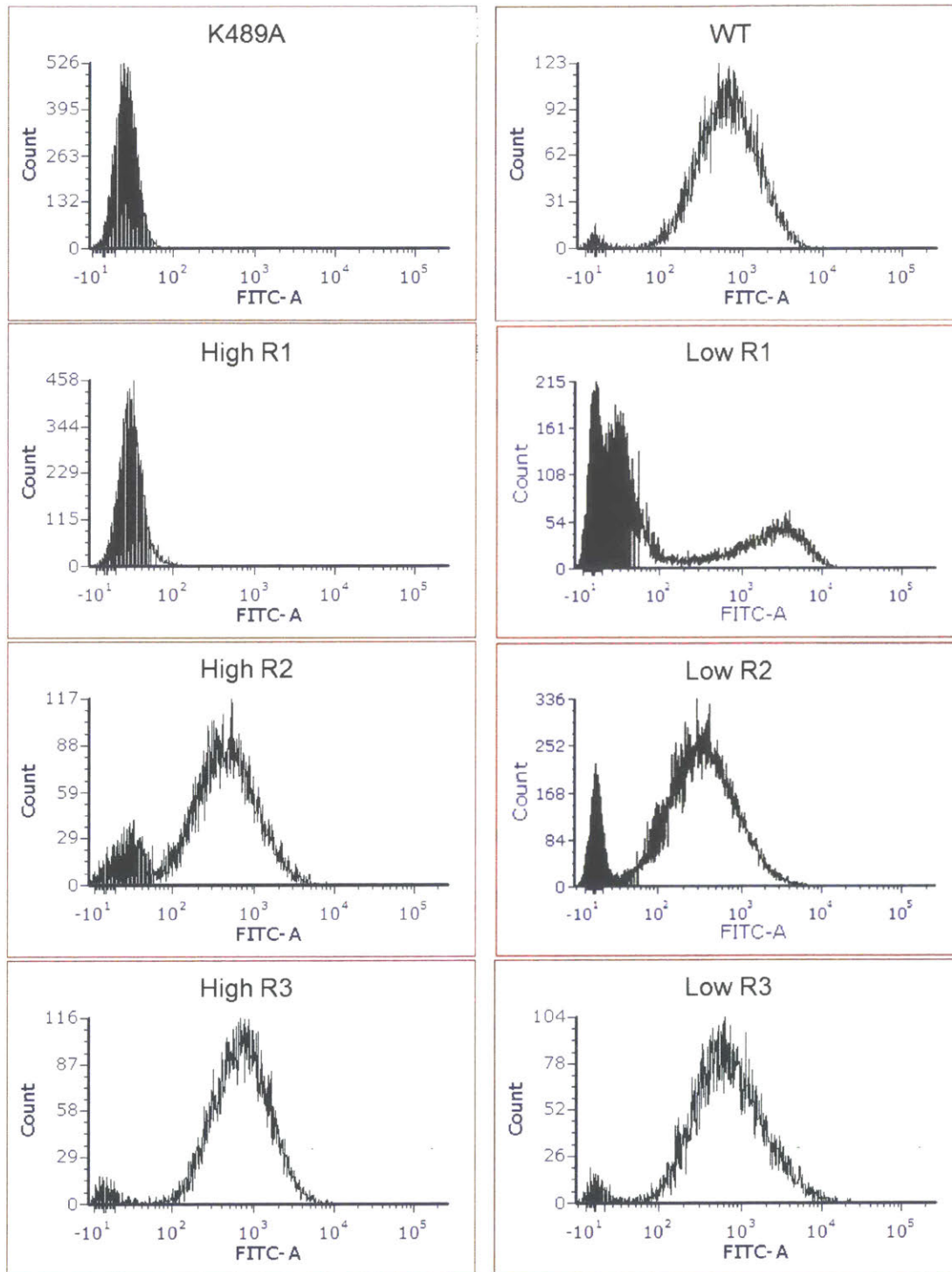
Figure 4.5. Population distributions of high and low mutation rate libraries. Number of events are plotted against GFP intensity (FITC-A). R1, R2, and R3 refer to the sorting rounds, where R1 is the initial library.

The hits that were not wild-type were cloned into a fresh vector and background strain without the sensor plasmid to remove any effects that might arise from non-MIPS mutations. Four of these hits demonstrated improved MI production (**Figure 4.6**A). To confirm that the amino acid change(s) were responsible for the increased titer, hits without the silent mutations were generated. In nearly all cases, the residue change led to improved production (**Figure 4.6**B). The single mutant I377T appeared to slightly hamper MIPS activity, although this deleterious effect was rescued by the top-performing V251I mutation. To determine whether the beneficial mutations were additive, a double mutant of Y250S and L321F was tested. While the Y250S / L321F mutations improved MI titer compared to wild-type (**Figure 4.6**B), the combination did not further improve titers compared to their single mutant counterparts.

Table 4.3. Hits from test and low mutation rate libraries. Sequence changes, MI titers, and fluorescence measurements from selected colonies isolated in each round of sorting. Colonies were selected for sequencing based on MI titer compared to a wild-type level cutoff value (see text). Silent refers to a codon (bp) change in that residue which did not result in an amino acid change.

Round	Clone	Mutations	Titer (g/L)	GFP / Biomass (a.u.)
Test	K3	Y250S / R225 Silent / P479 Silent	0.40	N/A
	WT		0.20	N/A
Low Round 2	B6	L321F / C399 Silent	0.71	2.26
	D4	L321F	0.75	2.78
	E5	L321F / C399 Silent	0.63	2.12
	WT		0.37	1.07
Low Round 3	A3	L321F	0.52	1.83
	B3	wt	0.52	1.63
	B4	wt	0.61	1.61
	C2	wt	0.54	0.60
	C3	wt	0.58	1.64
	C4	wt	0.77	1.54
	C5	wt	0.48	1.33
	D2	S79T, P277 Silent	0.55	2.49
	D3	wt	0.51	1.60
	D4	L134 Silent, L168 Silent, V251I, I377T	0.49	3.04
	D5	wt	0.53	2.48
	E3	Y486F	0.44	1.36
	E5	wt	0.43	1.42
	F4	wt	0.54	1.45
	F5	wt	0.53	0.88
	WT		0.08	0.06

Table 4.4. Hits from high mutation rate library. Sequence changes, MI titers, and fluorescence measurements from selected colonies isolated in each round of sorting. Colonies were selected for sequencing based on MI titer compared to a wild-type level cutoff value (see text). Silent refers to a codon (bp) change in that residue which did not result in an amino acid change.

Round	Clone	Mutations	Titer (g/L)	GFP / Biomass (a.u.)
High Round 1	A3	D390G	0.36	0.95
	A4	wt	0.37	0.85
	A5	wt	0.47	0.65
	A6	wt	0.49	0.33
	B3	V15 Silent, L305 Silent, S411 Silent, K468I	0.47	0.60
	C2	D338E, N355 Silent, H247Q, V467 Silent, T493 Silent, L526 Silent	0.45	0.70
	C4	V15 Silent, L305 Silent, S411 Silent, K468I	0.38	0.77
	WT		0.23	0.30
High Round 2	A8	wt	0.70	1.27
	B1	I9T	0.80	1.24
	C1	I9T	0.70	1.35
	C3	I9T	0.94	1.15
	C5	wt	0.81	1.10
	C6	wt	0.86	1.11
	D1	wt	0.65	2.20
	D3	I9T	0.74	1.62
	D7	I9T	0.72	0.86
	E1	wt	0.68	1.02
	E5	wt	0.76	1.76
	WT		0.85	1.21
High Round 3	A8	wt	0.76	0.99
	C8	wt	0.81	0.87
	D5	wt	0.62	1.48
	D6	wt	0.85	1.58
	E4	wt	0.65	1.25
	F4	wt	0.75	1.21
	F5	wt	0.79	1.31
	F7	wt	0.64	1.27
	WT		0.59	1.18
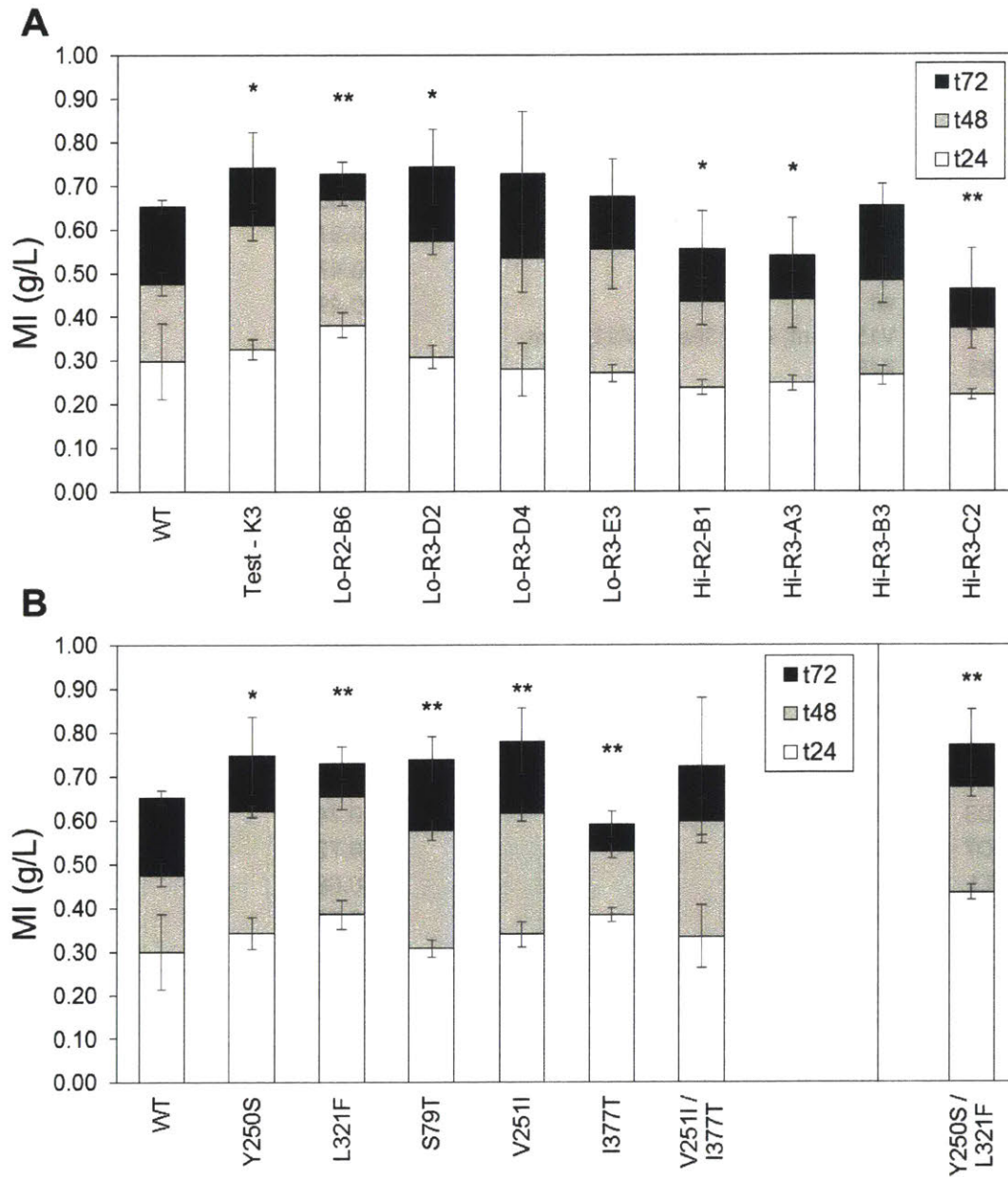
Figure 4.6. MI production from hits identified in FACS screening. (A) MI production from hits cloned into a fresh vector and background strain. (B) MI production from hits with only non-silent mutations and the Y250S / L321F mutant combination. Error bars denote ±1 S.D. from mean titers of five biological replicates. *p<0.1, **p<0.05 from paired two-tailed t-test.

4.4 Conclusions

In this study, a MI biosensor was used in a flow cytometry screen to efficiently test large libraries of MIPS mutants generated by error-prone PCR. The biosensor-based screen identified four MIPS mutants (Y250S, L321F, S79T, and V251I) that resulted in up to 20% increases in MI titer. While this improvement might not significantly increase glucaric acid titer due to limitations with MIOX, the second heterologous enzyme, these mutants can act as templates for further MIPS and pathway engineering efforts. The biosensor-based high-throughput screen enabled the use of powerful non-rational enzyme engineering methods for pathway improvement.

5. Conclusions and Outlook

5.1 Summary and Future Directions

In this work, we used a MI biosensor as both a genetic part for dynamic regulation and a high-throughput screen for directed evolution in order to improve glucaric acid production. The MI biosensor was constructed from *C. glutamicum* transcriptional regulator IpsA and made compatible in *E. coli* by promoter engineering. In this system, IpsA repressed expression from the engineered hybrid promoter except in the presence of MI. The biosensor could be adjusted and tuned for the different applications.

By coupling transcription of *Miox* to the presence of its substrate MI, the MI biosensor was used to dynamically control expression of *Miox*, a rate-controlling step in the glucaric-acid pathway, This MIOX regulation scheme was layered onto a glycolysis knockdown system, and the combination of the two systems improved glucaric acid production by 9-fold. Layered dynamic regulation demonstrates that controlled expression of pathway genes can significantly benefit production.

By inducing expression of *gfp* in the presence of MI, the MI biosensor facilitated high-throughput screening of a large library of MIPS by FACS. The FACS-based screen enabled the use of directed evolution, a powerful protein engineering method, to improve MIPS. The biosensor-based screen identified mutations in MIPS that improved MI production by up to 20%. Further work to elucidate the mechanisms by which these mutations improve production can be explored by measuring MIPS activity and performing *in silico* studies (e.g. homology modeling) of mutant

MIPS structures. It may also be interesting to generate analogous mutations in MIPS homologs to identify any key residues in the enzyme. Finally, while MIPS is a highly conserved enzyme, nature has provided numerous, diverse starting templates for MIPS. Directed evolution from a different sequence template might also unveil new beneficial mutations and key residues.

5.2 Outlook

5.2.1 Biosensors as Genetic Parts for Dynamic Regulation

Biosensors are the integral component for implementing dynamic pathway regulation, as they connect a signal to a response. Next generation dynamic regulation parts will likely rely on quorum sensing systems, which have the advantage of being pathway-independent[63,64]. Biosensors that detect a pathway-specific metabolite need to be identified, constructed, and tuned for each application, which can often be as complex as engineering the pathway. However, pathway-specific biosensors may be favored when there is already a well-characterized system on hand.

5.2.2 Biosensors for High-Throughput Screens

Biosensors have the potential to de-bottleneck the test phase in the metabolic engineering cycle. Their ability to serve as high-throughput screens can dramatically change how the design and build steps are executed. High-throughput screens enable the application of directed evolution strategies, which are often one-pot build methods. While initial pathway construction requires rational design and piecewise assembly of the pathway, evolution can accelerate the subsequent

optimization process by accessing increased sequence diversity. Even when rational design methods are used in conjunction with bio-foundries that leverage automated handling of multiple micro-titer plates in parallel, biosensor-based screening and selection can more rapidly test the designs than conventional analytics. In addition to the reduced run time of simple fluorescence or absorbance measurements versus chromatography, genetically encoded biosensors also possess the advantage of avoiding cell-medium separation or intracellular metabolite extraction steps. While biosensor-based screens will not replace conventional analytics, which are more quantitative and accurate, they will transform the design-build-test cycle.

5.2.3 Challenges of Deploying Biosensors in the Field

There are still many challenges in successfully implementing biosensors as high-throughput screens or parts for dynamic control. Quantification of the detected molecule input using fluorescence output signals is difficult. Signal processing of input to output is achieved with molecular interactions, which are non-linear. Relative differences in fluorescence do not map to the same differences in production. While identifying the needle in the haystack becomes a simple task, how similar the needle is to the hay is not quite as discernable.

Another significant challenge lies in identifying or engineering new biosensors for a desired molecule. Substantial efforts have been made to develop generalizable biosensor engineering methods. SELEX methods for identifying RNA aptamers that bind novel ligands[117], evolving

existing transcriptional regulators such as AraC[43], and engineering dCas9 for CRISPR interference or activation[65,118] have been demonstrated. It is difficult to evaluate the generalizability of these methods due to the many undocumented cases where these strategies have failed. Even with biosensor availability, the sensor may not be tuned for the relevant detection range, which varies by molecule, host, and stage in pathway development. Additional engineering is often required to re-calibrate the biosensor to behave properly. Currently, initial investment in developing the biosensor can be significant, demanding its own design-build-test cycle, and in certain cases narrowing down the design space or library size might be more efficient.

5.2.4 Biosensors beyond Metabolic Engineering

Despite limitations in their development, biosensors show promise for accelerating and transforming design-build-test cycles in metabolic engineering. Beyond microbial production, genetically encoded biosensors have been implemented as integral components of diagnostics[119], therapeutics[120], and agricultural applications[121].

As a detection device, biosensors have been used in biochemical assays, medical diagnostics, and quality control. In enzymatic assay development, biosensors can be introduced to supply readable measurements, reducing the need to couple additional reactions or synthesize colored chemical analogs. For example, the activity of O-methyl transferase variants were screened *in vitro* using the S-adenosyl-homocysteine biosensor[122]. As a diagnostic tool, biosensors have been engineered to specifically detect diseases such as Zika virus and produce a colorimetric readout

in response[119]. By lyophilizing the whole-cell biosensor and embedding it onto a small paper disc, this system can be easily transported, stored, and deployed in any location[119]. Microbes have also been employed to monitor wastewater quality by detecting toxic compounds such as heavy metals[123]. *Vibrio fischeri* was used as a high-throughput metal detector to identify samples whose contamination levels exceeded a certain threshold, reducing the number of samples required for screening by chromatography[124].

In the therapeutic area, the pharmaceutical company Synlogic has engineered the gut microbe *E. coli Nissle* to treat metabolic disorders such as phenylketonuria and hyperammonemia[120,125]. To treat phenylketonuria, the microbe was equipped with oxygen biosensors as regulatory components to perceive its approximate location in the digestive tract and appropriately control production of phenylalanine metabolizing enzymes[120]. The company also explored options where the therapeutic microbe would express genes involved in metabolizing ammonia upon detection of biomarkers for liver malfunction[125]. These strategies ensure that therapeutic agent is active only at the target location.

Finally, bacteria have also been engineered to aid nitrogen fixation in plants and improve agricultural output[121,126]. While most demonstrations of this technology have relied on constitutive expression of nitrogenase, the nitrogen fixing enzyme, biosensors can be used to induce nitrogenase expression under certain plant-associating conditions[121].

These applications demonstrate the versatility and potential of genetic parts that detect an input

and output a signal. Biosensors offer many opportunities as synthetic regulatory components and

screens in a variety of applications including and beyond metabolic engineering.

6. References

1. Cohen, S. N., Chang, A. C., Boyer, H. W. & Helling, R. B. Construction of biologically functional bacterial plasmids in vitro. *Proc. Natl. Acad. Sci. U. S. A.* **70,** 3240–4 (1973).

2. Bailey, J. E. Toward a science of metabolic engineering. *Science* **252,** 1668–75 (1991).

3. Nakamura, C. E. & Whited, G. M. Metabolic engineering for the microbial production of 1,3-propanediol. *Curr. Opin. Biotechnol.* **14,** 454–459 (2003).

4. Atsumi, S., Hanai, T. & Liao, J. C. Non-fermentative pathways for synthesis of branched-chain higher alcohols as biofuels. *Nature* **451,** 86–89 (2008).

5. Ro, D.-K. *et al.* Production of the antimalarial drug precursor artemisinic acid in engineered yeast. *Nature* **440,** 940–943 (2006).

6. Galanie, S., Thodey, K., Trenchard, I. J., Filsinger Interrante, M. & Smolke, C. D. Complete biosynthesis of opioids in yeast. *Science* **349,** 1095–100 (2015).

7. Luo, X. *et al.* Complete biosynthesis of cannabinoids and their unnatural analogues in yeast. *Nature* **567,** (2019).

8. Yim, H. *et al.* Metabolic engineering of Escherichia coli for direct production of 1,4-butanediol. *Nat. Chem. Biol.* **7,** 445–452 (2011).

9. Martin, C. H. *et al.* A platform pathway for production of 3-hydroxyacids provides a biosynthetic route to 3-hydroxy-γ-butyrolactone. *Nat. Commun.* **4,** 1414 (2013).

10. Nielsen, J. & Keasling, J. D. Engineering Cellular Metabolism. *Cell* **164,** 1185–1197 (2016).

11. Woolston, B. M., Edgar, S. & Stephanopoulos, G. Metabolic engineering: past and future. *Annu. Rev. Chem. Biomol. Eng.* **4,** 259–88 (2013).

12. Wheeler, D. L. *et al.* Database resources of the National Center for Biotechnology Information. *Nucleic Acids Res.* **35,** D5–D12 (2007).

13. Kanehisa, M. & Goto, S. KEGG: kyoto encyclopedia of genes and genomes. *Nucleic Acids Res.* **28,** 27–30 (2000).

14. UniProt: a worldwide hub of protein knowledge. *Nucleic Acids Res.* **47,** D506–D515 (2019).

15. Salis, H. M., Mirsky, E. A. & Voigt, C. A. Automated design of synthetic ribosome binding sites to control protein expression. *Nat. Biotechnol.* **27,** 946–950 (2009).

16. Copeland, W. B. *et al.* Computational tools for metabolic engineering. *Metab. Eng.* **14,** 270–280 (2012).

17. Nielsen, A. A. K. *et al.* Genetic circuit design automation. *Science* **352,** aac7341 (2016).

18. Casini, A., Storch, M., Baldwin, G. S. & Ellis, T. Bricks and blueprints: methods and standards for DNA assembly. *Nat. Rev. Mol. Cell Biol.* **16,** 568–576 (2015).

19. Jakočiūnas, T., Jensen, M. K. & Keasling, J. D. CRISPR/Cas9 advances engineering of microbial cell factories. *Metab. Eng.* **34,** 44–59 (2015).

20. Marchione, M. Chinese researcher claims first gene-edited babies. *AP exclusive* (2018). at <https://www.apnews.com/4997bb7aa36c45449b488e19ac83e86d>

21. Marcellin, E. & Nielsen, L. K. Advances in analytical tools for high throughput strain engineering. *Curr. Opin. Biotechnol.* **54,** 33–40 (2018).

22. Zhang, F. & Keasling, J. Biosensors and their applications in microbial metabolic engineering. *Trends Microbiol.* **19,** 323–9 (2011).

23. Dietrich, J. A., McKee, A. E. & Keasling, J. D. High-throughput metabolic engineering: advances in small-molecule screening and selection. *Annu. Rev. Biochem.* **79,** 563–90 (2010).

24. Salis, H., Tamsir, A. & Voigt, C. A. *Bacterial Sensing and Signaling. Bacterial Sensing and Signaling* **16,** (S. Karger AG, 2009).

25. Liu, Y., Liu, Y. & Wang, M. Design, Optimization and Application of Small Molecule Biosensor in Metabolic Engineering. *Front. Microbiol.* **8,** 2012 (2017).

26. Wang, Q., Tang, S.-Y. & Yang, S. Genetic biosensors for small-molecule products: Design and applications in high-throughput screening. *Front. Chem. Sci. Eng.* **11,** 15–26 (2017).

27. Carpenter, A. C., Paulsen, I. T. & Williams, T. C. Blueprints for Biosensors: Design, Limitations, and Applications. *Genes (Basel).* **9,** (2018).

28. De Paepe, B., Peters, G., Coussement, P., Maertens, J. & De Mey, M. Tailor-made transcriptional biosensors for optimizing microbial cell factories. *J. Ind. Microbiol. Biotechnol.* **44,** 623–645 (2017).

29. Hallberg, Z. F., Su, Y., Kitto, R. Z. & Hammond, M. C. Engineering and In Vivo Applications of Riboswitches. *Annu. Rev. Biochem.* 515–539 (2017). at <https://doi.org/10.1146/annurev-biochem- 060815-014628>

30. Winkler, W., Nahvi, A. & Breaker, R. R. Thiamine derivatives bind messenger RNAs directly to regulate bacterial gene expression. *Nature* **419,** 952–956 (2002).

31. Win, M. N. & Smolke, C. D. Higher-order cellular information processing with synthetic RNA devices. *Science* **322,** 456–60 (2008).

32. Wang, J. X., Lee, E. R., Morales, D. R., Lim, J. & Breaker, R. R. Riboswitches that Sense S-adenosylhomocysteine and Activate Genes Involved in Coenzyme Recycling. *Mol. Cell* **29,** 691–702 (2008).

33. Uchiyama, T. & Miyazaki, K. Product-induced gene expression, a product-responsive reporter assay used to screen metagenomic libraries for enzyme-encoding genes. *Appl. Environ. Microbiol.* **76,** 7029–35 (2010).

34. Levskaya, A. *et al.* Synthetic biology: engineering Escherichia coli to see light. *Nature* **438,**

441–2 (2005).

35.   Fernandez-Rodriguez, J., Moser, F., Song, M. & Voigt, C. A. Engineering RGB color vision into Escherichia coli. *Nat. Chem. Biol.* (2017). at <https://www.nature.com/nchembio/journal/vaop/ncurrent/pdf/nchembio.2390.pdf>

36.   Fernandez-López, R., Ruiz, R., de la Cruz, F. & Moncalián, G. Transcription factor-based biosensors enlightened by the analyte. *Front. Microbiol.* **6,** 648 (2015).

37.   Ang, J., Harris, E., Hussey, B. J., Kil, R. & McMillen, D. R. Tuning response curves for synthetic biology. *ACS Synth. Biol.* **2,** 547–67 (2013).

38.   Engstrom, M. D. & Pfleger, B. F. Transcription control engineering and applications in synthetic biology. *Synth. Syst. Biotechnol.* **2,** 176–191 (2017).

39.   Merulla, D. & van der Meer, J. R. Regulatable and Modulable Background Expression Control in Prokaryotic Synthetic Circuits by Auxiliary Repressor Binding Sites. *ACS Synth. Biol.* **5,** 36–45 (2015).

40.   Schendzielorz, G. *et al.* Taking Control over Control: Use of Product Sensing in Single Cells to Remove Flux Control at Key Enzymes in Biosynthesis Pathways. *ACS Synth. Biol.* **3,** 21–29 (2014).

41.   Xu, P., Li, L., Zhang, F., Stephanopoulos, G. & Koffas, M. Improving fatty acids production by engineering dynamic pathway regulation and metabolic control. *Proc. Natl. Acad. Sci. U. S. A.* **111,** 11299–304 (2014).

42.   Liu, D., Evans, T. & Zhang, F. Applications and advances of metabolite biosensors for metabolic engineering. *Metab. Eng.* (2015). doi:10.1016/j.ymben.2015.06.008

43.   Tang, S.-Y., Fazelinia, H. & Cirino, P. C. AraC regulatory protein mutants with altered effector specificity. *J. Am. Chem. Soc.* **130,** 5267–5271 (2008).

44.   Chan, C. T. Y., Lee, J. W., Cameron, D. E., Bashor, C. J. & Collins, J. J. 'Deadman' and 'Passcode' microbial kill switches for bacterial containment. *Nat. Chem. Biol.* **12,** 82–86 (2016).

45.   Juárez, J. F., Lecube-Azpeitia, B., Brown, S. L., Johnston, C. D. & Church, G. M. Biosensor libraries harness large classes of binding domains for construction of allosteric transcriptional regulators. *Nat. Commun.* **9,** 3101 (2018).

46.   de Los Santos, E. L. C., Meyerowitz, J. T., Mayo, S. L. & Murray, R. M. Engineering Transcriptional Regulator Effector Specificity Using Computational Design and In Vitro Rapid Prototyping: Developing a Vanillin Sensor. *ACS Synth. Biol.* (2015). doi:10.1021/acssynbio.5b00090

47.   Tang, S. Y. & Cirino, P. C. Design and application of a mevalonate-responsive regulatory protein. *Angew. Chemie - Int. Ed.* **50,** 1084–1086 (2011).

48.   Tang, S.-Y. *et al.* Screening for enhanced triacetic acid lactone (TAL) production by

recombinant Escherichia coli expressing a designed TAL reporter. *J. Am. Chem. Soc.* (2013). doi:10.1021/ja402654z

49. Chen, W. *et al.* Design of an ectoine-responsive AraC mutant and its application in metabolic engineering of ectoine biosynthesis. *Metab. Eng.* **30,** 149–55 (2015).

50. Frei, C. S., Qian, S. & Cirino, P. C. New engineered phenolic biosensors based on the AraC regulatory protein. *Protein Eng. Des. Sel.* **31,** 213–220 (2018).

51. Zaslaver, A. *et al.* Just-in-time transcription program in metabolic pathways. *Nat. Genet.* **36,** 486–491 (2004).

52. Venayak, N., Anesiadis, N., Cluett, W. R. & Mahadevan, R. Engineering metabolism through dynamic control. *Curr. Opin. Biotechnol.* **34,** 142–152 (2015).

53. Xu, P. Production of chemicals using dynamic control of metabolic fluxes. *Curr. Opin. Biotechnol.* **53,** 12–19 (2018).

54. Holtz, W. J. & Keasling, J. D. Engineering static and dynamic control of synthetic pathways. *Cell* **140,** 19–23 (2010).

55. Gadkar, K. G., Doyle III, F. J., Edwards, J. S. & Mahadevan, R. Estimating optimal profiles of genetic alterations using constraint-based models. *Biotechnol. Bioeng.* **89,** 243–251 (2005).

56. Farmer, W. R. & Liao, J. C. Improving lycopene production in Escherichia coli by engineering metabolic control. *Nat. Biotechnol.* **18,** 533–7 (2000).

57. Zhang, F., Carothers, J. M. & Keasling, J. D. Design of a dynamic sensor-regulator system for production of chemicals and fuels derived from fatty acids. *Nat. Biotechnol.* **30,** 354–9 (2012).

58. Dahl, R. H. *et al.* Engineering dynamic pathway regulation using stress-response promoters. *Nat. Biotechnol.* **31,** 1039–46 (2013).

59. Xu, P. *et al.* Design and kinetic analysis of a hybrid promoter-regulator system for malonyl-CoA sensing in Escherichia coli. *ACS Chem. Biol.* **9,** 451–8 (2014).

60. Solomon, K. V, Sanders, T. M. & Prather, K. L. J. A dynamic metabolite valve for the control of central carbon metabolism. *Metab. Eng.* **14,** 661–671 (2012).

61. Tan, S. Z., Manchester, S. & Prather, K. L. J. Controlling central carbon metabolism for improved pathway yields in Saccharomyces cerevisiae. *ACS Synth. Biol.* (2015). doi:10.1021/acssynbio.5b00164

62. Brockman, I. M. & Prather, K. L. J. Dynamic knockdown of E. coli central metabolism for redirecting fluxes of primary metabolites. *Metab. Eng.* **28,** 104–113 (2014).

63. Gupta, A., Reizman, I. M. B., Reisch, C. R. & Prather, K. L. J. Dynamic regulation of metabolic flux in engineered bacteria using a pathway-independent quorum-sensing circuit. *Nat. Biotechnol.* **35,** 1–27 (2017).

64.   Soma, Y. & Hanai, T. Self-induced metabolic state switching by a tunable cell density sensor for microbial isopropanol production. *Metab. Eng.* **30,** 7–15 (2015).

65.   Zalatan, J. G. *et al.* Engineering complex synthetic transcriptional programs with CRISPR RNA scaffolds. *Cell* **160,** 339–50 (2015).

66.   Cobb, R. E., Chao, R. & Zhao, H. Directed evolution: Past, present, and future. *AIChE J.* **59,** 1432–1440 (2013).

67.   You, L. & Arnold, F. H. *Directed evolution of subtilisin E in Bacillus subtilis to enhance total activity in aqueous dimethylformamide. Protein Engineering* **9,** (1994).

68.   Stemmer, W. P. C. Rapid evolution of a protein in vitro by DNA shuffling. *Nature* **370,** 389–391 (1994).

69.   Schallmey, M., Frunzke, J. & Eggeling, L. Looking for the pick of the bunch: high-throughput screening of producing microorganisms with biosensors. *Curr. Opin. Biotechnol.* **26,** 148–154 (2014).

70.   Eggeling, L., Bott, M. & Marienhagen, J. Novel screening methods—biosensors. *Curr. Opin. Biotechnol.* **35,** 30–36 (2015).

71.   Dietrich, J. A., Shis, D. L., Alikhani, A. & Keasling, J. D. Transcription factor-based screens and synthetic selections for microbial small-molecule biosynthesis. *ACS Synth. Biol.* **2,** 47–58 (2013).

72.   Kortmann, M., Mack, C., Baumgart, M. & Bott, M. Pyruvate Carboxylase Variants Enabling Improved Lysine Production from Glucose Identified by Biosensor-Based High-Throughput Fluorescence-Activated Cell Sorting Screening. *ACS Synth. Biol.* **8,** 274–281 (2019).

73.   Michener, J. K. & Smolke, C. D. High-throughput enzyme evolution in Saccharomyces cerevisiae using a synthetic RNA switch. *Metab. Eng.* **14,** 306–16 (2012).

74.   Seok, J. Y. *et al.* Directed evolution of the 3-hydroxypropionic acid production pathway by engineering aldehyde dehydrogenase using a synthetic selection device. *Metab. Eng.* **47,** 113–120 (2018).

75.   Werpy, T. A., Holladay, J. E. & White, J. F. *Top Value Added Chemicals From Biomass: I. Results of Screening for Potential Candidates from Sugars and Synthesis Gas.* (2004). doi:10.2172/926125

76.   Grand View Research. *Glucaric Acid Market Size & Share | Global Industry Report, 2018-2025.* (2017). at <https://www.grandviewresearch.com/industry-analysis/glucaric-acid-market>

77.   Moon, T. S., Yoon, S.-H., Lanza, A. M., Roy-Mayhew, J. D. & Prather, K. L. J. Production of glucaric acid from a synthetic pathway in recombinant Escherichia coli. *Appl. Environ. Microbiol.* **75,** 589–95 (2009).

78.   Shiue, E., Brockman, I. M. & Prather, K. L. J. Improving product yields on D-glucose in

Escherichia coli via knockout of pgi and zwf and feeding of supplemental carbon sources. *Biotechnol. Bioeng.* **112,** 579–87 (2015).

79. Qu, Y.-N. *et al.* Biosynthesis of D-glucaric acid from sucrose with routed carbon distribution in metabolically engineered Escherichia coli. *Metab. Eng.* **47,** 393–400 (2018).

80. Moon, T. S., Dueber, J. E., Shiue, E. & Prather, K. L. J. Use of modular, synthetic scaffolds for improved production of glucaric acid in engineered E. coli. *Metab. Eng.* **12,** 298–305 (2010).

81. Shiue, E. & Prather, K. L. J. Improving d-glucaric acid production from myo-inositol in E. coli by increasing MIOX stability and myo-inositol transport. *Metab. Eng.* **22,** 22–31 (2014).

82. Zheng, S. *et al.* One-pot two-strain system based on glucaric acid biosensor for rapid screening of myo-inositol oxygenase mutations and glucaric acid production in recombinant cells. *Metab. Eng.* **49,** 212–219 (2018).

83. Rogers, J. K. & Church, G. M. Genetically encoded sensors enable real-time observation of metabolite production. *Proc. Natl. Acad. Sci. U. S. A.* 1600375113- (2016). doi:10.1073/pnas.1600375113

84. Guay, L. M. Pathway and Protein Engineering for Improved Glucaric Acid Production in Escherichia coli by. (MIT, 2019).

85. Baumgart, M. *et al.* IpsA, a novel LacI-type regulator, is required for inositol-derived lipid formation in Corynebacteria and Mycobacteria. *BMC Biol.* **11,** 122 (2013).

86. Registry of Standard Biological Parts. at <http://www.partsregistry.org/>

87. Dhamankar, H., Tarasova, Y., Martin, C. H. & Prather, K. L. J. Engineering E. coli for the biosynthesis of 3-hydroxy-γ-butyrolactone (3HBL) and 3,4-dihydroxybutyric acid (3,4-DHBA) as value-added chemicals from glucose as a sole carbon source. *Metab. Eng.* **25,** 72–81 (2014).

88. Shiue, E. Improvement of D-glucaric acid production in Escherichia coli. (MIT, 2014). at <http://dspace.mit.edu/handle/1721.1/87132>

89. Quan, J. & Tian, J. Circular polymerase extension cloning. *Methods Mol. Biol.* **1116,** 103–117 (2014).

90. Dhamankar, H. H. Engineering E. coli for the biosynthesis of 3-hydroxy-γ-butyrolactone (3HBL) and 3,4-dihydroxybutyric acid (3,4-DHBA) as value-added chemicals from glucose as a sole carbon source. (MIT, 2013).

91. Collado-Vides, J., Magasanik, B. & Gralla, J. D. Control site location and transcriptional regulation in Escherichia coli. *Microbiol. Mol. Biol. Rev.* **55,** 371–394 (1991).

92. Cox, R. S., Surette, M. G. & Elowitz, M. B. Programming gene expression with combinatorial promoters. *Mol. Syst. Biol.* **3,** 145 (2007).

93. Xu, P., Rizzoni, E. A., Sul, S.-Y. & Stephanopoulos, G. Improving Metabolic Pathway

Efficiency by Statistical Model-Based Multivariate Regulatory Metabolic Engineering. *ACS Synth. Biol.* acssynbio.6b00187 (2016). doi:10.1021/acssynbio.6b00187

94.   Brockman, I. M. & Prather, K. L. J. Dynamic metabolic engineering: New strategies for developing responsive cell factories. *Biotechnol. J.* **10**, 1360–9 (2015).

95.   Li, Z., Kessler, W., van den Heuvel, J. & Rinas, U. Simple defined autoinduction medium for high-level recombinant protein production using T7-based Escherichia coli expression systems. *Appl. Microbiol. Biotechnol.* **91**, 1203–1213 (2011).

96.   Bothfeld, W., Kapov, G. & Tyo, K. E. J. A Glucose-Sensing Toggle Switch for Autonomous, High Productivity Genetic Control. *ACS Synth. Biol.* acssynbio.6b00257 (2017). doi:10.1021/acssynbio.6b00257

97.   Reizman, I. M. B. *et al.* Improvement of glucaric acid production in E. coli via dynamic control of metabolic fluxes. *Metab. Eng. Commun.* **2**, 109–116 (2015).

98.   Calvo, J. M. & Matthews, R. G. The leucine-responsive regulatory protein, a global regulator of metabolism in Escherichia coli. *Microbiol. Rev.* **58**, 466–90 (1994).

99.   Schleif, R. Regulation of the l-arabinose operon of Escherichia coli. *Trends Genet.* **16**, 559–565 (2000).

100.   Shen-Orr, S. S., Milo, R., Mangan, S. & Alon, U. Network motifs in the transcriptional regulation network of Escherichia coli. *Nat. Genet.* **31**, 64–68 (2002).

101.   Gardner, T. S., Cantor, C. R. & Collins, J. J. Construction of a genetic toggle switch in Escherichia coli. *Nature* **403**, 339–42 (2000).

102.   Soma, Y., Tsuruno, K., Wada, M., Yokota, A. & Hanai, T. Metabolic flux redirection from a central metabolic pathway toward a synthetic pathway using a metabolic toggle switch. *Metab. Eng.* **23**, 175–184 (2014).

103.   FEEDAP. Scientific Opinion on the safety and efficacy of inositol as a feed additive for fish, dogs and cats. *EFSA J.* **12**, (2014).

104.   Chad A. Hansen, Amy B. Dean, K. M. Draths, and & Frost*, J. W. Synthesis of 1,2,3,4-Tetrahydroxybenzene from d-Glucose: Exploiting myo-Inositol as a Precursor to Aromatic Chemicals. (1999). doi:10.1021/JA9840293

105.   Jin, X. & Geiger, J. H. Structures of NAD + - and NADH-bound 1- L - myo -inositol 1-phosphate synthase. *Acta Crystallogr. Sect. D Biol. Crystallogr.* **59**, 1154–1164 (2003).

106.   You, C. *et al.* An in vitro synthetic biology platform for the industrial biomanufacturing of myo-inositol from starch. *Biotechnol. Bioeng.* **114**, 1855–1864 (2017).

107.   Dean-Johnson, M. & Henrye, S. A. Biosynthesis of Inositol in Yeast PRIMARY STRUCTURE OF MYO-INOSITOL-1-PHOSPHATE SYNTHASE (EC 5.5.1.4) AND FUNCTIONAL ANALYSIS OF ITS STRUCTURAL GENE, THE INOI LOCUS*. *J. Biol. Chem.* **264**, 1274–1283 (1989).

108.   Stein, A. J. & Geiger, J. H. The Crystal Structure and Mechanism of 1L- myo-Inositol-1-

phosphate Synthase *. *JBC Pap. Press. Publ. January* **277,** 9484–9491 (2002).

109. Geiger, J. H. & Jin, X. in *Biology of Inositols and Phosphoinositides* 157–180 (Springer US, 2006). doi:10.1007/0-387-27600-9_7

110. Fujisawa, T., Fujinaga, S. & Atomi, H. An In Vitro Enzyme System for the Production of myo-Inositol from Starch. *Appl. Environ. Microbiol.* **83,** (2017).

111. Kniewel, R. *et al.* Structural analysis of Saccharomyces cerevisiae myo-inositol phosphate synthase. *J. Struct. Funct. Genomics* **2,** 129–134 (2002).

112. Ghoshdastidar, K., Chatterjee, A., Chatterjee, A. & Majumder, A. L. in *Biology of Inositols and Phosphoinositides* (eds. Majumder, A. L. & Biswas, B. B.) 313–338 (Springer, 2006). at <https://link.springer.com/content/pdf/10.1007/0-387-27600-9_13.pdf>

113. Majumder, A. L., Chatterjee, A., Ghosh Dastidar, K. & Majee, M. Diversification and evolution of L - *myo* -inositol 1-phosphate synthase [1]. *FEBS Lett.* **553,** 3–10 (2003).

114. Merulla, D., Hatzimanikatis, V. & van der Meer, J. R. Tunable reporter signal production in feedback-uncoupled arsenic bioreporters. *Microb. Biotechnol.* **6,** 503–14 (2013).

115. Neelon, K., Wang, Y., Stec, B. & Roberts, M. F. Probing the mechanism of the Archaeoglobus fulgidus inositol-1-phosphate synthase. *J. Biol. Chem.* **280,** 11475–82 (2005).

116. Drummond, D. A., Iverson, B. L., Georgiou, G. & Arnold, F. H. Why High-error-rate Random Mutagenesis Libraries are Enriched in Functional and Improved Proteins. doi:10.1016/j.jmb.2005.05.023

117. Ellington, A. D. & Szostak, J. W. In vitro selection of RNA molecules that bind specific ligands. *Nature* **346,** 818–822 (1990).

118. Bikard, D. *et al.* Programmable repression and activation of bacterial gene expression using an engineered CRISPR-Cas system. *Nucleic Acids Res.* **41,** 7429–37 (2013).

119. Pardee, K. *et al.* Rapid, Low-Cost Detection of Zika Virus Using Programmable Biomolecular Components. *Cell* **165,** 1255–1266 (2016).

120. Isabella, V. M. *et al.* Development of a synthetic live bacterial therapeutic for the human metabolic disease phenylketonuria. *Nat. Biotechnol.* **36,** 857–864 (2018).

121. Geddes, B. A. *et al.* Use of plant colonizing bacteria as chassis for transfer of N2-fixation to cereals. *Curr. Opin. Biotechnol.* **32,** 216–222 (2015).

122. Su, Y., Hickey, S. F., Keyser, S. G. L. & Hammond, M. C. *In Vitro* and *In Vivo* Enzyme Activity Screening via RNA-Based Fluorescent Biosensors for *S* -Adenosyl- l -homocysteine (SAH). *J. Am. Chem. Soc.* **138,** 7040–7047 (2016).

123. Bereza-Malcolm, L. T., Mann, G. & Franks, A. E. Environmental Sensing of Heavy Metals Through Whole Cell Microbial Biosensors: A Synthetic Biology Approach. *ACS Synth. Biol.* **4,** 535–546 (2015).

124. Farré, M. I., García, M.-J., Tirapu, L., Ginebreda, A. & Barceló, D. Wastewater toxicity screening of non-ionic surfactants by Toxalert® and Microtox® bioluminescence inhibition assays. *Anal. Chim. Acta* **427,** 181–189 (2001).

125. Falb, D., Isabella, V. M., Kotula, J. W., Miller, P. F. & Machinani, S. Bacteria engineered to treat diseases associated with hyperammonemia. (2017). at <http://rstb.>

126. Cocking, E. C. D. SYSTEMIC NON-NODULAR ENDOSYMBIOTIC NITROGEN FIXATION IN PLANTS. (2012). at <https://patentimages.storage.googleapis.com/fd/6c/de/ef457b36539595/US8137665.pdf>